Study of Zinc Cobalt ferrite nanoparticles and Zinc Cobalt ferrite /Graphene oxide nanocomposites for Methylene blue dye adsorption

A Dissertation for
PHY-651 Discipline Specific Dissertation
Credits: 16
Submitted in partial fulfillment of Masters Degree

M.Sc in Physics
Goa University
In the subject of Physics

by

Akshada Ankush Naik Gaonkar
22P0430001
ABC ID:151-615-391-555
201908123

Under the supervision of
Dr.Pranav P. Naik

School Of Physical and Applied Science
Physics discipline

Goa University
May 2024

Examined by:

Seal of the School

DECLARATION

I hereby declare that the data presented in this Dissertation / Internship report entitled, "Study of Graphene Oxide-Ferrite nanocomposite for Dye degradation." is based on the results of investigations carried out by me in the Physics Discipline at the School of Physical and Applied Sciences, Goa University under the Supervision of Dr. Pranav Naik and the same has not been submitted elsewhere for the award of a degree or diploma by me. Further, I understand that Goa University or its authorities will be not be responsible for the correctness of observations / experimental or other findings given in the dissertation. I hereby authorize the University authorities to upload this dissertation on the dissertation repository or anywhere else as the UGC regulations demand and make it available to any one as needed.

Akaonkar

Name: Ms. Akshada Naik Gaonkar

Roll no: 22P0430001

Discipline: Physics

School of Physical and Applied Sciences

Date: 08/05/2024

Place: Goa University

COMPLETION CERTIFICATE

This is to certify that the dissertation / internship report "Study of Zinc Cobalt ferrite nanoparticles and Zinc Cobalt ferrite /Graphene oxide nanocomposites for Methylene blue dye adsorption" is a bonafide work carried out by Ms.Akshada Naik Gaonkar under my supervision in partial fulfilment of the requirements for the award of the degree of M.Sc in Physics at the School of Physical and Applied Sciences, Goa University.

Supervisor: Dr.Pranav Naik 8/5/2024

Physics

Date: 08/05/2024

Dean: Prof. Ramesh V.Pai

Physics

School of Physical and Applied Sciences

Date: 08/05/2024

Place: Goa University

School of Physical and Applied Sciences Goa University

ACKNOWLEDGEMENT

I extend my sincere gratitude to my project guide Dr.Pranav P. Naik for his guidance and support throughout the entire Dissertation work. I would like to thank Prof. Dr. Ramesh V Pai, Dean of School of Physical and Applied Sciences for giving me an opportunity to carry out my dissertation work. I would like to express my gratitude to the research Scholar Ms. Sugania Chandavelou for her constant help and support throughout the project. Heartfelt thanks to the non-teaching staff of the Physics Discipline, especially for their timely help in the laboratory. I extend my heartfelt gratitude to Goa University for providing the necessary resources, facilities, and academic environment which have greatly facilitated the completion of this thesis. I am indebted to my family for their enduring encouragement, understanding, and unwavering belief in my abilities throughout this academic pursuit. Their support has been a source of strength and motivation

Contents

1 INTRODUCTION **2**

1.1 Nanomaterial 2

1.2 Spinel Ferrite 3

1.3 Ferrites in nanoform 5

1.4 Graphene Oxide 6

1.5 Ferrite/Graphene Oxide nanocomposite 7

1.6 Degradation of Methylene blue dye 8

1.7 Aim of the project 9

2 LITEATURE REVIEW **10**

3 Method of Preparation **19**

3.1 Synthesis of **Zinc Cobalt ferrite** through **Hydrothermal method**. 21

3.2 Synthesis of **Graphene oxide** through **Modified Hummer's method**. 22

3.3 Synthesis of **Zinc Cobalt ferrite Graphene oxide** through **Hydrothermal method**. 23

4 Characterization Techniques **24**

4.1 X-Ray diffraction (XRD) 24

4.2 UV-Vis spectroscopy 26

4.3 Raman Spectroscopy 27

4.4 Scanning Electron Microscopy (SEM) 28

4.5 Dielectric measurement 30

5 Results and Discussion **32**

5.1 X-Ray Diffraction (XRD) 32

5.2 Raman Spectroscopy 35

5.3 Scanning electron microscopy 37
5.4 Dielectric Spectroscopy 38
5.5 Adsorption of Methylene blue dye 39

List of Figures

1.1 Size comparison of living and nonliving beings. 2

1.2 Color dependence on size of gold particles. 3

1.3 Band gap dependence on size. 3

1.4 Spinel ferrite structure. 4

1.5 Graphene oxide 6

3.1 Synthesis of Zinc Cobalt ferrite through Hydrothermal method 21

3.2 Synthesis of Graphene oxide through Modified Hummer's method 22

3.3 Synthesis of Zinc Cobalt ferrite Graphene oxide through Modified Hummer's method 23

4.1 Schematic diagram of X-ray diffraction 24

4.2 X-ray diffraction setup 25

4.3 Schematic diagram of UV-Vis Spectroscopy 26

4.4 Schematic diagram Raman scattering 28

4.5 Schematic diagram of Scanning Electron Microscopy 29

4.6 Scanning Electron Microscopy setup 29

5.1 XRD pattern of (a) $Zn_{0.2}Co_{0.8}Fe_2O_4$, (b) $Zn_{0.5}Co_{0.5}Fe_2O_4$, (c) $Zn_{0.8}Co_{0.2}Fe_2O_4$. 32

5.2 XRD pattern of Graphene oxide. 33

5.3 XRD pattern of (d) $Zn_{0.2}Co_{0.8}Fe_2O_4$/GO (e) $Zn_{0.5}Co_{0.5}Fe_2O_4$/GO (f) $Zn_{0.8}Co_{0.2}Fe_2O_4$/GO 33

5.4 Rietveld refinement of (a) $Zn_{0.2}Co_{0.8}Fe_2O_4$, (b) $Zn_{0.5}Co_{0.5}Fe_2O_4$, (c) $Zn_{0.8}Co_{0.2}Fe_2O_4$ and (d) $Zn_{0.2}Co_{0.8}Fe_2O_4$/GO(7.5%) , (e) $Zn_{0.5}Co_{0.5}Fe_2O_4$/GO(7.5%) , (f) $Zn_{0.8}Co_{0.2}Fe_2O_4$/GO(7.5%) 34

5.5 Variations of Lattice constant 'a' and Crystallite size 't' and Strain 'ϵ' with increasing Cobalt concentration 35

5.6 Raman Spectra of (a) $Zn_{0.2}Co_{0.8}Fe_2O_4$, (b) $Zn_{0.5}Co_{0.5}Fe_2O_4$, (c) $Zn_{0.8}Co_{0.2}Fe_2O_4$ 35

5.7 Raman Spectra of Graphene oxide 36

5.8 Raman Spectra of (d) $Zn_{0.2}Co_{0.8}Fe_2O_4$/GO(7.5%) (e) $Zn_{0.5}Co_{0.5}Fe_2O_4$/GO(7.5%) (f) $Zn_{0.8}Co_{0.2}Fe_2O_4$/GO(7.5%) 36

5.9 Scanning electron microscopy images of (a) $Zn_{0.2}Co_{0.8}Fe_2O_4$, (b) $Zn_{0.5}Co_{0.5}Fe_2O_4$, (c) $Zn_{0.8}Co_{0.2}Fe_2O_4$ (d) $Zn_{0.2}Co_{0.8}Fe_2O_4$/GO(7.5%) (e) $Zn_{0.5}Co_{0.5}Fe_2O_4$/GO(7.5%) (f) $Zn_{0.8}Co_{0.2}Fe_2O_4$/GO(7.5%) 37

5.10 Dielectric constant as a function of frequency 38

5.11 Adsorption of Methylene blue dye 39

Abstract

The present study is focused on structural, morphological, dielectric properties of Zinc Cobalt ferrite nanoparticles and Zinc Cobalt ferrite /Graphene oxide nanocomposites. The Zinc Cobalt ferrite nanoparticles were synthesized using hydrothermal method, Graphene oxide was synthesized using modified Hummer's method which was used to synthesize Zinc Cobalt ferrite /Graphene oxide nanocomposites using hydrothermal method. These were characterized using X-ray diffraction (XRD) for structural properties. The morphological study was done using scanning electron microscope. Raman spectroscopy was used to study the vibrational modes present and to confirm the formation of graphene oxide along with ferrites in the nanocomposites. Dielectric measurements were done to study dielectric constant of all the samples. Lastly, the adsorption of Methylene blue dye was studied , in which it is seen that the dye removal by the Zinc Cobalt ferrite nanoparticles is approximately 38% and dye removal by the Zinc Cobalt ferrite/ Graphene oxide nanocomposite is nearly 60%.

Chapter 1

INTRODUCTION

1.1 Nanomaterial

Nanotechnology involves the synthesis and application of materials at incredibly small scales, typically on the order of a billionth of a meter (10^{-9} meters). These materials are classified as ultrafine particles, as shown in fig.1.1, which illustrates the size comparison of nanoparticles with various living and nonliving species. Nanoparticles exhibit unique properties distinct from their bulk counterparts, including changes in electronic structure, reactivity, and thermal and mechanical properties when they reach the nanoscale. Jose Varghese et al. (2019)

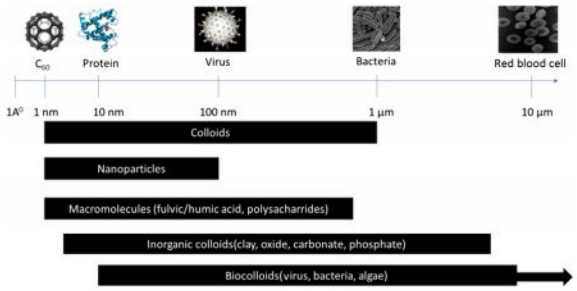

Figure 1.1: Size comparison of living and nonliving beings.
Jose Varghese et al. (2019)

By harnessing nanotechnology, we can create materials and devices with precise control at the level of individual atoms and molecules. Over the past two decades, there have been significant advancements in the design of colloids and nanoparticles, both by mimicking nature and through synthetic methods. The size of nanoparticles greatly influences their properties. While there isn't much difference in properties between a particle in its bulk state and its microscale size, significant changes occur when the particle size decreases to less than 100 nm. At this scale, quantum size effects become dominant and dictate properties such as chemical, thermal, mechanical, optical,

electrical, and magnetic behaviors.

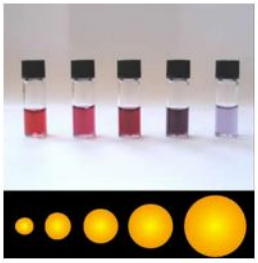

Figure 1.2: Color dependence on size of gold particles.
Jose Varghese et al. (2019)

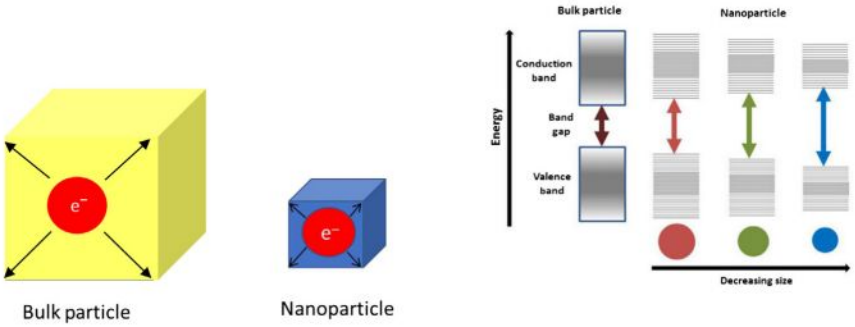

Figure 1.3: Band gap dependence on size.
Jose Varghese et al. (2019)

The size-dependent properties of gold nanoparticles (AuNPs) have been extensively studied in recent decades, as shown in Fig.1.2, which depicts the size-dependent color of AuNPs. At the nanoscale, gold particles exhibit a purple color, unlike their bulk form, which is yellow. This color change is attributed to the shift in their band type from continuous to discrete due to the confinement effect, as depicted in Fig.1.3.

These quantum effects in the nanoscale are fundamental to the "tunability" of properties. By simply adjusting the particle size, we can alter the material property of interest, such as fluorescence. Jose Varghese et al. (2019)

1.2 Spinel Ferrite

Spinel ferrites are a type of material with the chemical formula $M[Fe_2]O_4$, where M represents a divalent metal ion such as Fe, Co, Ni, Mn, Mg, or Zn. These ferrites have a structure based on a face-centered cubic (FCC) lattice, where oxygen anions form a closely packed array and metal cations occupy interstitial positions. Pacakova et al. (2017)

The structure of spinel ferrites is typically represented as MM'_2X_4, where M and M' represent cations coordinated tetrahedrally and octahedrally, respectively, and X is an anion, usually oxygen

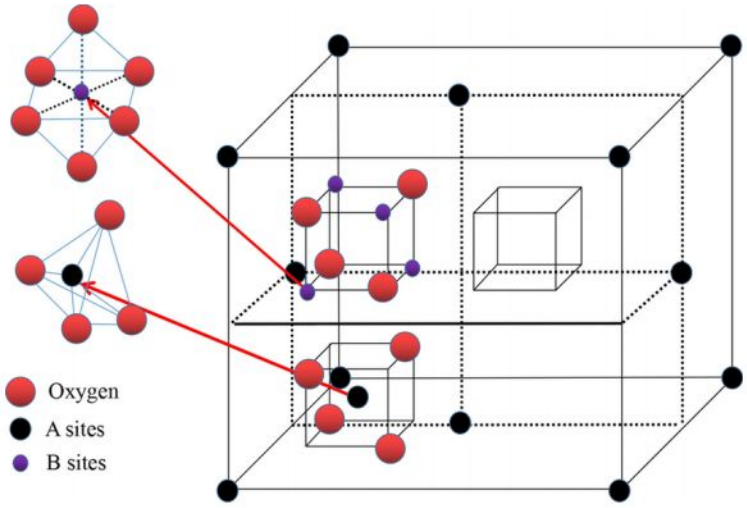

Figure 1.4: Spinel ferrite structure.
Yu et al. (2020)

or fluorine. In spinel ferrites, M is a divalent metal ion, while M' is Fe^{3+}, which can occupy either tetrahedral or octahedral sites. SOUFI et al. (2021)

There are two types of spinel structures: normal and inverse. In a normal spinel, the divalent metal ions occupy tetrahedral sites, while Fe^{3+} occupies octahedral sites. In contrast, in an inverse spinel, half of the Fe^{3+} ions occupy tetrahedral sites, and the other half share octahedral sites with the divalent metal ions. SOUFI et al. (2021)

The magnetic properties of spinel ferrites are influenced by the distribution of cations between tetrahedral and octahedral sites, as well as the nature of the metal ions themselves. Ferrites with a normal spinel structure can exhibit either ferrimagnetic or antiferromagnetic behavior, depending on the magnetic moments of the metal ions. Conversely, ferrites with an inverse spinel structure are typically ferrimagnetic, with a net magnetic moment resulting from the unequal magnetic moments of the cations at tetrahedral and octahedral sites. Pham et al. (2020)

Spinel ferrites (SFs) are categorized into three main types based on the distribution of cations at the tetrahedral (A) and octahedral (B) sites within their crystal lattice. This classification is primarily determined by the degree of inversion, denoted as x, which represents the fraction of M^{2+} ions occupying octahedral sites. The general chemical formula for SFs is$M[Fe_2]O_4$, where M represents a divalent metal ion.

1. Normal Spinel Ferrites: In normal SFs, the divalent cations M^{2+} occupy tetrahedral (A) sites, while the trivalent cations Fe^{3+} are located at octahedral (B) sites. The structural formula for normal SFs is $M^{2+}](A)[Fe^{2+}{}_2Fe^{3+}](B){O_4}^{2-}$. Examples of normal SFs include $ZnFe_2O_4$ and $CdFe_2O_4$.

2. Inverse Spinel Ferrites: In inverse SFs, the divalent cations M^{2+} occupy octahedral (B)

sites, while half of the trivalent cations Fe^{3+} are placed in tetrahedral (A) sites, and the other half share the octahedral sites with the divalent metal ions. The structural formula for inverse SFs is $[Fe^{3+}](A)[M^{2+}Fe^{3+}](B){O_4}^{2-}$. Examples of inverse SFs include Fe_3O_4, $CoFe_2O_4$, $NiFe_2O_4$, $CuFe_2O_4$, and $MgFe_2O_4$.

3. Mixed Spinel Ferrites: In mixed spinel ferrites, both the divalent cations M^{2+} and trivalent cations Fe^{3+} ions are distributed at both tetrahedral (A) and octahedral (B) sites within the crystal lattice. The structural formula for mixed SFs is similar to that of normal SFs, but with a distribution of both cations at both sites. An example of a mixed SF is $MnFe_2O_4$.

It's worth noting that the value of x (in the range $0 < x < 1$) can vary depending on the synthesis method and the specific constituents of the ferrites. For instance, $CuFe_2O_4$ can exhibit either inverse or mixed spinel structure depending on the synthesis conditions. The distribution of cations in SFs significantly influences their physical, chemical, and magnetic properties, making them important materials in various technological applications. SOUFI et al. (2021)

1.3 Ferrites in nanoform

Nanostructured ferrites possess distinctive characteristics that set them apart, including their abundant natural availability, cost-effectiveness, remarkable catalytic prowess, expansive surface area, selectivity, surface oxygen mobility, electrical conductivity, and robust thermal, mechanical, and chemical stability. Moreover, their magnetic attributes facilitate effortless separation from reaction mediums, adding to their appeal. These exceptional properties render nanostructured ferrites highly appealing for a diverse array of applications. These applications span across water treatment, high-density storage devices, sensors, semiconductor photocatalysts, ferrofluids, hyperthermia, magnetic resonance imaging, magnetic separation, drug delivery, biosensing, cancer treatment, audio and videotapes, photo-detectors, and antibacterial applications. Physicochemical attributes further enhance their utility, featuring elevated Curie temperatures, significant magneto crystalline anisotropy, commendable thermal resilience, superb magnetic qualities, customizable size and shape, substantial specific surface area, active surface sites, enduring chemical stability, and straightforward modification or functionalization. These properties are intricately influenced by factors like the composition of divalent cations within the spinel structure, their distribution across tetrahedral and octahedral sites, synthesis techniques, grain size, morphology, and annealing conditions. SOUFI et al. (2021)

Nanostructured ferrites find application across a diverse spectrum, serving as magnetic materials, adsorbents for eliminating heavy metals and dyes from water, catalysts and photocat-

alysts for pollutant eradication, contrast agents, hyperthermia agents, drug delivery platforms, sensors/biosensors in medical and biotechnological domains, electronic components, microwave devices, electromagnetic interference shields, and recording media. These multifaceted applications are made possible by the distinctive attributes of nanostructured ferrites, including their exceptional stability, cost-effectiveness in preparation, outstanding physicochemical properties, elevated catalytic efficacy, and effortless recovery and reusability. SOUFI et al. (2021)

1.4 Graphene Oxide

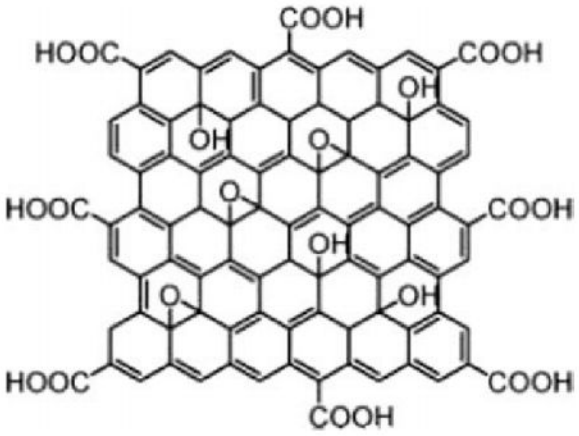

Figure 1.5: Graphene oxide
Gerani et al. (2016)

Graphene oxide (GO) is a material derived from the oxidation and exfoliation of layered crystalline graphite, resulting in a single-atom-thick carbon layer with oxygen-containing functional groups on both surfaces. Within GO particles, pristine graphene domains exist, the abundance and size of which are influenced by the specifics of the preparation process. Remarkably hydrophilic, GO forms stable aqueous dispersions as well as dispersions in diverse organic solvents. Its surface offers numerous chemical avenues for attaching functional groups, enabling precise control over optical transparency, electrical conductivity, and thermal conductance. Such versatility renders GO suitable for a broad spectrum of applications, particularly those emphasizing electrical conductivity, chemical functionality, and mechanical strength. Dideikin and Vul (2019)

Graphene oxide, consisting of a single layer of sp2 carbon atoms, showcases distinct vibrational modes such as C=O, C=C from unoxidized sp2 CC bonds, and C-O vibrations. Through chemical reduction, it transforms into chemically converted graphene (CCG), with some residual defects, yet retaining a partially restored graphitic structure and adjustable electrical conductivity. Reduction by hydrazine vapor yields reduced graphene materials with thicknesses between 1 to 3 nm, ideal

for device fabrication. This material serves as a robust and flexible membrane, allowing for facile modification or functionalization of its carbon backbone, thus enabling the cost-effective production of graphene-based materials at a large scale. Marcano et al. (2010) Zhu et al. (2010)

Graphene oxide (GO) has a honeycomb lattice structure and is characterized by an abundance of reactive oxygen functional groups, giving a porous nature. Its attributes as a low-cost, non-toxic, and effective modifier make it highly regarded in various applications. Furthermore, GO has demonstrated the adsorption capacities of magnetic nanoparticles, elevating its potential for a wide array of applications Ghobadi et al. (2018). The high specific surface area of graphene oxide (GO), stemming from the hydrophilic functional groups decorating its sheets, renders it well-suited for a multitude of applications, particularly adsorption processes Sadighian et al. (2018).

1.5 Ferrite/Graphene Oxide nanocomposite

The Zinc ferrite-graphene oxide nanocomposite has exhibited remarkable efficacy in removing dyes from water, displaying a high adsorption capacity for organic dyes. Its recyclability and magnetic characteristics enhance its potential as an adsorbent for treating dye-contaminated wastewater. Sadighian et al. (2018). The ferrite graphene oxide nanocomposite has a large theoretical surface area and impressive adsorption capacity, because of its abundance of reactive oxygen functional groups.The presence of graphene oxide gives the nanocomposite superparamagnetic properties, with a saturation magnetization of 35.5 emu/g, facilitating rapid and cost-effective magnetic separation processes. The nanocomposite achieves a maximum adsorption capacity of 1001 mg/g for La^{3+} and 982 mg/g for Ce^{3+}.Ghobadi et al. (2018). Combining graphene oxide with metal ferrites yields nanocomposites with distinctive properties. These metal ferrite graphene oxide nanocomposites demonstrate heightened stability in aqueous and polar solvents, attributed to the hydrophilic nature of GO's oxygen-containing functional groups. Leveraging GO's substantial surface area, these composites prove effective in pollutant adsorption. These nanocomposites exhibit enhanced adsorption capabilities, with the NiFe2O4@GO composite particularly for its superior efficiency, owing to its specific surface area and mesopore structure. Bayantong et al. (2021b). The Manganeese ferrite graphene oxide nanocomposite displayed a saturation magnetism (Ms) of 28.8 emu/g, indicating superparamagnetic behavior due to the incorporation of magnetic ferrite onto the graphene oxide substrate. Furthermore, the nanocomposite exhibited an elevated degree of defect, as evidenced by the ID/IG ratio of 1.13, attributed to the interaction between the oxygen groups present in graphene oxide and the manganese ferrite nanoparticles. Regarding adsorption capabilities, the MnFe2O4/GO nanocomposite showcased an increased adsorption capacity for

Pb^{2+} ions and NR dye with escalating pollutant concentrations, reaching levels of up to 625 mg/g for Pb^{2+} ions and 90 mg/g for NR dye. Notably, the nanocomposite displayed robust removal efficiencies for both pollutants, ranging from 39% to 98.8% for Pb^{2+} ions and 63% to 94% for NR dye.Katubi et al. (2021)

The NiFe2O4@GO nanocomposites showcase remarkable conductivity and adsorption properties, primarily attributed to the inclusion of graphene oxide . GO plays a pivotal role in enhancing the separation of charge carriers and serves as an electron sink. Moreover, the presence of NiFe2O4 nanoparticles on the GO surface facilitates the selective adsorption of dye molecules via π stacking interactions with aromatic rings, thereby augmenting the photocatalytic activity of the nanocomposites.Bayantong et al. (2021a)

1.6 Degradation of Methylene blue dye

Dyes used in various industries, such as textiles and manufacturing, often contain harmful chemicals that can seep into our water sources. Once these dyes enter our waterways, they can have detrimental effects on aquatic life and ecosystems, disrupting the delicate balance of our environment. The pollution caused by dye not only impacts water quality but also poses risks to human health, as these chemicals can find their way into our food chain. Furthermore, the disposal of dye waste without proper treatment can lead to long-lasting environmental damage, affecting not only the present but future generations as well. It is neccessary that industries take responsibility for their dye usage and implement sustainable practices to mitigate the harmful effects of dye pollution. One of the main contributors to water pollution is the textile industry, which extensively uses various types of dyes in the production process. These dyes can be categorized into two main types: natural dyes and synthetic dyes . Natural dyes are derived from plants, insects, or minerals, and are considered more environmentally friendly compared to synthetic dyes. Synthetic dyes are manufactured from chemical compounds and have been placed on a high pedestal in the textile industry due to their improved colour fastness, varied range of pigments and easy application as compared to natural dyes. However, they have been identified to be harmful to the environment and human health by researchers. When effluent containing harmful chemicals like sodium sulphide is discharged into the environment improperly, they cause a lot of diseases and hinder smooth air flow. Fobiri (2022)

This approch intends to decrease the discharge of significant amounts of methylene blue (MB) dyes by textile industries into natural water sources which poses a threat to both human health and microbial communities. MB is highly toxic and non-biodegradable, with carcinogenic properties,

posing serious risks to human health and detrimental effects on the environment. Exposure to MB can lead to a range of health issues, including respiratory distress, abdominal disorders, blindness, digestive and mental disorders, nausea, diarrhea, vomiting, cyanosis, shock, gastritis, jaundice, methemoglobinemia, tissue necrosis, increased heart rate, skin/eye irritations, skin redness, and itching. The observed adverse effect level (NOAEL) for MB in rats is reported to be 25 mg kg^{-1}. The discharge of MB into the environment not only poses toxic threats but also reduces light penetration, acts as a toxic supply to food chains for organisms, and results in the formation of highly colored sub-products even at low concentrations. Furthermore, MB's high molar absorption coefficient reduces sunlight transmittance, affecting oxygen solubility, photosynthetic activity of aquatic life, and the diversity of the biological community. Khan et al. (2022)

1.7 Aim of the project

In the above sections we have seen the ill effects of MB dye onto the environment. This approach intends to prepare Zinc Cobalt ferrite-Graphene oxide nanocomposite, to be used as an adsorbent of Methylene blue dye (adsorbate).

- Synthesis of $Zn_xCo_{1-x}Fe_2O_4$ nanoparticles and $Zn_xCo_{1-x}Fe_2O_4$/GO nanocomposites through Hydrothermal method. (x=0.2, 0.5, 0.8)
- Characterization using X-Ray Diffraction, Raman spectroscopy, Scanning electron microscopy, Dielectric measurements.
- Study the adsorption capacity of the $Zn_xCo_{1-x}Fe_2O_4$ nanoparticles and $Zn_xCo_{1-x}Fe_2O_4$/GO nanocomposites for Methylene blue dye.

Chapter 2

LITEATURE REVIEW

Bayantong et al. (2021b) developed MFe_2O_4@GO where M being the metals Cu, Co, Ni through solution combustion method.These adsorbents were characterised to study surface area, pore diameter, surface functional groups, elemental composition.The Langmuir isotherm model was found to better fit the adsorption of methylene blue onto MFe2O4@GO, suggesting monolayer adsorption behavior. The kinetic data indicated that the adsorption process followed the pseudo-second-order model, indicating that chemical adsorption governed the removal of methylene blue using MFe_2O_4@GO. $NiFe_2O_4$/GO exhibited maximum adsorption capacity compared to $CoFe_2O_4$/GO and $CuFe_2O_4$/GO. The BET analysis of the metal ferrite nano-enabled graphene oxide (MFe_2O_4@GO) composites revealed high specific surface areas and mesopore volumes, indicating their porous nature and large surface area. $NiFe_2O_4$@GO composite exhibited the highest adsorption performance among the investigated graphene oxide-metal ferrites due to its high specific surface area and presence of mesopores.

In the study by Lan Huong et al. (2018), investigated the impact of graphene oxide (GO) concentration on the properties and adsorption activity of $MnFe_2O_4$ nanoparticles and GO-$MnFe_2O_4$ nanocomposites. Various characterization techniques, including TEM, HRTEM, XRD, FTIR, VSM, XPS, and BET, were employed to analyze the nanocomposites. Batch experiments were conducted to study the adsorption behavior of arsenic(V) ions and methylene blue dye on the nanocomposites. The results indicated that increasing GO concentration enhanced the adsorption efficiency of the nanocomposites, with the pseudo-second-order model providing good fits for all samples. The Langmuir and Freundlich isotherm models were used to analyze adsorption behavior, showing high adsorption capacities for both MB dye and arsenic(V) ions. Overall, the enhanced adsorption mechanisms were mainly attributed to increased electrostatic interactions and active

binding sites as the GO content increased.

In the year 2018, Sadighian et al. (2018) focused on the development and application of zinc ferrite and graphene oxide nanocomposite for the removal of dye from water. The nanocomposites were synthesized using facile hydrothermal method. The researchers characterised the prepared nanocomposites using various techniques like Fourier infrared spectroscopy (FT-IR), X-Ray diffraction (XRD), scanning electron microscopy (SEM) to study it's structure, morphology, chemical composition. The batch adsorption experiments demonstrated the efficiency of the nanocomposites to adsorb methyl orange . Also studied effect of pH, initial dye concentration, temperature, contact time to understand it's kinetics and thermodynamics. In the degradation experiment 20 mg of nanocomposite (adsorbent) was added to the dye solution. After 20 minutes of contact time between the adsorbent and the dye solution (adsorbate), adsorption equilibrium was reached. It was seen that as the amount of added adsorbent increased, dye removal was also seen to increase. In the kinetic studies, the pseudo second order kinetic model and Langmuir model were well fitted which concludes that adsorption is chemical adsorption and monolayer.The key findings were,nanocomposite exhibited superior adsorption capabilities compared to zinc ferrite nanoparticles alone. Kinetics, isotherm, and regeneration/desorption studies showed that the prepared adsorbents could be reused for the application.

Study by Sidhaarth et al. (2018), investigates the use of cobalt ferrite nanoparticles as an adsorbent to eliminate Congo red dye from aqueous solutions. The nanoparticles were synthesized using the co-precipitation method. Analysis via X-Ray diffraction and Transmission electron microscopy confirmed the formation of single-phase cobalt ferrite nanoparticles ranging in size from 16 to 60nm. The X-ray diffraction analysis revealed that the resulting product is $CoFe_2O_4$, with inverse spinal structure. Presence of single phase $CoFe_2O_4$ with face centered cubic structure was confirmed. SEM analysis revealed that the $CoFe_2O_4$ nanoparticles exhibit a uniform, monodisperse spherical morphology characterized by a narrow particle size distribution, also noticed agglomeration. TEM analysis indicated that the nanoparticle structure was agglomerated, resulting in a cloudy appearance under alkaline conditions. These cobalt ferrite nanoparticles were tested for their efficacy in removing color from synthetic wastewater. In the batch studies effect of contact time, adsorbent dosage, pH of the dye solution, initial concentration of dye, agitation speed were analysed. Removal efficiency of 98% was achieved with an optimal contact time of 130 minutes, an adsorbent dosage of 0.10 g/50ml, a pH of 4, and an initial dye concentration of 60 mg/L, at a stirring speed of 150 rpm. Both Langmuir and Temkin isotherms provided good fits, indicating homogeneous multilayer adsorption.

Baynosa et al. (2020)In the study, a magnetically separable mesoporous composite of $ZnFe_2O_4$ nanoparticles and reduced graphene oxide was synthesized through an eco-friendly hydrothermal method for efficient photocatalytic degradation of methylene blue (MB) dye under solar radiation. The composite exhibited high photocatalytic performance attributed to its enhanced adsorptivity, extended light absorption, and improved separation efficiency of photoinduced charges. The addition of reduced graphene oxide contributed to increased light absorption and charge separation, leading to higher efficiency in dye degradation. The nanocomposite displayed a pseudo-first-order reaction for dye degradation, with a higher rate constant for methylene blue compared to rhodamine B. Characterization of the nanocomposite through various techniques such as Raman spectroscopy, FT-IR spectroscopy, XPS, SEM, and HRTEM confirmed the reduction of graphene oxide, the presence of $ZnFe_2O_4$ phase, and the interaction between $ZnFe_2O_4$ nanoparticles and graphene sheets. The nanocomposite exhibited good crystallinity and high photocatalytic activity. Characterization techniques, including X-ray diffraction, BET analysis, thermogravimetric analysis, UV-vis spectroscopy, and various spectroscopic methods, provided insights into the structural and functional properties of the photocatalyst samples. Overall, the study demonstrated the efficacy of the mesoporous zinc ferrite@reduced graphene oxide nanocomposite as a promising photocatalyst for efficient dye degradation under solar radiation.

Bayantong et al. (2021a) $NiFe_2O_4$@GO was effectively synthesized using the solution combustion method. Under UV light, it exhibits remarkable photocatalytic activity attributed to the conductivity of graphene oxide, facilitating charge carrier stabilization and separation, thereby reducing recombination. This synergy enables a 'hook and destroy' mechanism, enhancing pollutant degradation by improving adsorption and overcoming mass transport limitations. Nearly complete decolorization occurs within 120 minutes of UV irradiation, even at a low catalyst dose of 0.5 g/L. The optimal concentration for efficient photodegradation is 0.04 mM, as higher concentrations prolong operational times due to limited photon transport in highly colored solutions. Graphene oxide (GO) in the $NiFe_2O_4$@GO nanocomposites enhances photocatalytic properties by promoting charge carrier separation, acting as an electron sink, and facilitating selective adsorption of dye molecules through π stacking interactions with aromatic rings. The impact of competing ions, particularly carbonate, on photocatalytic degradation kinetics was investigated, with carbonate identified as the main factor decelerating the process. Radical scavenging experiments highlight the significant role of photogenerated holes and hydroxyl radicals as primary reactive oxidant species.

The degradation of methylene blue dye (MB) through photocatalysis was explored using manganese ferrite ($MnFe_2O_4$) nanoparticles alone and in combination with reduced graphene oxide (rGO) to form heterostructures (MnFe2O4/rGO) under UV light by Mandal et al. (2020). The MnFe2O4 nanoparticles, synthesized via a simple co-precipitation method, exhibited a single-phase cubic spinel structure and superparamagnetic properties. The $MnFe_2O_4$/rGO heterostructures demonstrated the attachment of sphere-like $MnFe_2O_4$ nanoparticles onto rGO nanosheets, resulting in reduced agglomeration. Comparative analysis revealed that $MnFe_2O_4$/rGO exhibited enhanced photocatalytic activity compared to bare $MnFe_2O_4$ nanoparticles. Under UV irradiation for 290 minutes, MB degradation reached 84% with $MnFe_2O_4$, while with $MnFe_2O_4$/rGO heterostructures, 97% degradation occurred in just 60 minutes. This improvement was supported by fitting the Langmuir-Hinshelwood Kinetics equation. The superior photocatalytic performance of the heterostructure was primarily attributed to the decrease in the recombination process of photogenerated charge carriers. Hydroxyl radicals were identified as crucial in the $MnFe_2O_4$-graphene system for MB photodegradation. Thus, $MnFe_2O_4$ nanoparticles-decorated reduced graphene oxide heterostructures hold promise as photocatalysts for the degradation of harmful organic dyes in water.

This study by Singh et al. (2016) focuses on exploring the adsorption potential of cobalt ferrite nanoparticles synthesized using the combustion method and modified with an SDS surfactant for the removal of a cationic dye, crystal violet. The nanoparticles were characterized using techniques such as FTIR, SEM, and XRD analysis. Batch adsorption experiments were conducted to investigate the removal of crystal violet dye by the SDS-coated cobalt ferrite nanoparticles. Various parameters such as initial dye concentration, contact time, adsorbent dose, and pH were studied at a constant temperature. The equilibrium time for adsorption was found to be 2 hours. The results showed that the adsorption percentage of the dye increased with an increase in the adsorbent dose and initial dye concentration. Additionally, basic pH conditions exhibited better results compared to acidic pH. The Langmuir adsorption isotherm provided the best fit, followed by Temkin, Freundlich, and Dubinin-Raduskevich isotherms. The monolayer adsorption capacity was determined to be 105 mg/g, comparable to other reported adsorbents. Kinetic studies revealed that adsorption followed the Lagergren pseudo-second-order kinetics model better than other models such as Lagergren pseudo-first order and Elovich. Furthermore, adsorption studies conducted at different temperatures indicated that adsorption increased with increasing temperature, suggesting an endothermic sorption phenomenon. Thermodynamic analysis using the Van't Hoff equation revealed that the adsorption mechanism involved both physical and chemical adsorption processes, with enthalpy values ranging from 23 to 88 kJ/mol for different concentrations. Overall, the study

provides valuable insights into the adsorption behavior of SDS-coated cobalt ferrite nanoparticles for crystal violet dye removal, highlighting their potential for water treatment applications.

Adel et al. (2021). This study focuses on using mesoporous magnesium ferrite nanoparticles, synthesized via the sol-gel method, for removing indigo carmine dye from wastewater. The nanoparticles' physicochemical properties were thoroughly analyzed using various techniques such as FESEM, EDX, XPS, XRD, HRTEM, SAED, FTIR, Zeta potential, VSM, and BET analysis. The researchers investigated and optimized several experimental parameters affecting the adsorption process, including contact time, adsorbent dose, solution temperature, and pH. Different adsorption isotherms were studied to understand the mechanism of anionic dye removal. Thermodynamic parameters revealed that the dye removal process was endothermic, and there was a random arrangement of indigo carmine molecules on the adsorbent particles. The mesoporous $MgFe_2O_4$ nano-adsorbent showed a surface area of 28.8 m2/g, an average particle size of 34 nm, and a narrow pore volume. It exhibited an adsorption capacity of 46 mg/g and maintained high stability even after four cycles of regeneration and reuse. Overall, the findings highlight the potential of mesoporous magnesium ferrite nanoparticles as efficient and reusable adsorbents for removing indigo carmine dye from aqueous solutions, offering insights into the adsorption mechanism and stability of the nanoparticles.

Das et al. (2021). This study evaluates the effectiveness of magnesium ferrite nanoparticles (MgF-NPs) as an adsorbent for removing malachite green (MG) dye from water, particularly under ultrasonic irradiation. The MgF-NPs have a specific surface area of 70.266 m2/g and a pore volume of 0.311 cc/g, with an average pore diameter of 7.354 nm. The optimal solution pH for MG dye adsorption with ultrasonication is found to be 8.0, which is favorable for large-scale field application. The ultrasonication-assisted adsorption process achieves over 90% MG dye removal within just 15 minutes due to enhanced mass transfer. In contrast, using overhead stirring or shaking as mixing methods reduces the dye removal efficacy to 70% and 65%, respectively. The adsorption kinetics follow the pseudo-second-order model, and the equilibrium isotherm analysis conforms to the Langmuir model, indicating a maximum monolayer adsorption capacity of 487.60 mg/g. The presence of chloride ions in the solution hinders MG dye removal efficiency from 91% to 67%, while the presence of nitrate, sulfate, and phosphate ions has minimal effect on dye removal efficacy. Cost analysis for synthesizing MgF-NPs suggests a cost of 50.88 USD/kg of adsorbent, which is economical for large-scale industrial applications. Overall, the study demonstrates that magnesium ferrite nanoparticles, particularly under ultrasonic irradiation, are effective and economically viable adsorbents for removing malachite green dye from aqueous solutions, providing valuable insights for water treatment applications.

Mahmoodi (2013) This paper focuses on the synthesis of magnetic zinc ferrite ($ZnFe_2O_4$) nanoparticles and their application in the photocatalytic degradation of dyes from colored wastewater. Specifically, Reactive Red 198 (RR198) and Reactive Red 120 (RR120) were used as model dyes for the study. The characteristics of the synthesized $ZnFe_2O_4$ nanoparticles were investigated using Fourier transform infrared (FTIR), X-ray diffraction (XRD), and scanning electron microscopy (SEM) techniques. The photocatalytic dye degradation ability of $ZnFe_2O_4$ nanoparticles was studied using UV-vis spectrophotometry and ion chromatography (IC). The study evaluated the effects of ZnFe2O4 dosage, initial dye concentration, and the presence of salts on dye degradation. The results revealed that $ZnFe_2O_4$ nanoparticles exhibited efficient photocatalytic activity in degrading dyes from colored wastewater. Intermediate aliphatic products such as formate, acetate, and oxalate anions were detected during the degradation process. Additionally, inorganic anions such as nitrate and sulfate were identified as products of dye mineralization. Overall, the findings suggest that $ZnFe_2O_4$ nanoparticles can serve as effective magnetic photocatalysts for the degradation of dyes in colored wastewater, offering potential applications in water treatment and environmental remediation.

López et al. (2021) This study focuses on creating multifunctional materials for degrading dyes found in textile industry effluents. The design involves $Co0.25Zn0.75Fe_2O_4$ ferrite nanoparticles with super-paramagnetic behavior, acting as seeds in the Stöber process to form spherical SiO2 particles. The SiO2 acts as a template, mechanically stabilizing the $Co0.25Zn0.75Fe_2O_4$ ferrite to prevent particle agglomeration and maintain super-paramagnetic behavior. Subsequently, the SiO2 beads are coated with a ZnO ultrathin layer using atomic layer deposition (ALD) technique. The synthesized materials are thoroughly characterized for their morphology, size, composition, magnetic response, and photocatalytic activity using various techniques. The final $Co0.25Zn0.75Fe_2O_4$ nanostructured material exhibits good mechanical stability, excellent magnetic response, and high efficiency in catalyzing the degradation of toxic red amaranth dye under UV irradiation. Overall, the results demonstrate that these materials are effective photocatalysts and can be efficiently recovered from wastewater using magnetic separation protocols. This approach offers promising prospects for the treatment of wastewater contaminated with textile dyes, contributing to both environmental protection and resource recovery.

Ghobadi et al. (2018) In recent years, the increasing use of rare earth elements (REEs) has led to their release into industrial wastewater, posing significant environmental challenges. To address this issue, this study focuses on recycling rare earth cations (La_{3+} and Ce_{3+}) from aqueous solutions using $MnFe_2O_4$-graphene oxide ($MnFe_2O_4$-GO) magnetic nanoparticles. The synthesized nanoparticles were comprehensively characterized using various techniques such as XRD, FE-SEM, FT-IR, Raman spectroscopy, VSM, BET, and DLS. The adsorption isotherms, kinetics, thermodynamics, and desorption of REEs on MnFe2O4-GO were investigated. The maximum adsorption capacity for La_{3+} and Ce_{3+} under optimal conditions (room temperature and pH = 7) was found to be 1001 mg/g and 982 mg/g, respectively, with complete reactions occurring within 20 minutes. The adsorption data fitted well with the Langmuir model, and the kinetics followed the pseudo-second order model. Thermodynamic analysis indicated that the adsorption reactions were endothermic and spontaneous, while the Dubinin-Radushkevich model suggested chemical ion-exchange adsorption. Desorption studies demonstrated the regenerability of $MnFe_2O_4$-GO for multiple reuses. Overall, $MnFe_2O_4$-GO exhibited high adsorption capacity, chemical stability, reusability, fast kinetics, easy magnetic separation, and a simple synthesis method, making it a high-performance adsorbent for REEs.

Katubi et al. (2021) These studies highlight the potential of nanocomposites for water treatment, targeting pollutants like Pb2+ ions and NR dye. The synthesized $MnFe_2O_4$/GO nanocomposite was thoroughly characterized, and its optimal conditions for adsorption were determined through various factors such as initial concentration, dose, pH, and contact time.The results showed that increasing pollutant concentrations led to higher adsorption capacities, with Pb2+ ions reaching 625 mg/g and NR dye reaching 90 mg/g. Additionally, higher adsorbent doses improved removal efficiency, and the optimum pH for adsorption was found to be 6.0. The kinetics of adsorption indicated rapid initial adsorption followed by gradual saturation, with optimum contact times determined to be 120 and 30 minutes for Pb2+ ions and NR dye, respectively.The adsorption mechanism was concluded to be monolayer adsorption based on Langmuir fitting, with adsorption capacities of 636.94 mg/g for Pb2+ ions and 46.08 mg/g for NR dye. Furthermore, the nanocomposite demonstrated reusability and stability over five cycles, reducing overall treatment costs.Similarly, in the study focusing on recycling rare earth cations using $MnFe_2O_4$-GO nanoparticles, the synthesized nanoparticles exhibited high adsorption capacities for La3+ and Ce3+, with complete reactions occurring within 20 minutes under optimal conditions. The nanocomposite also showed chemical stability, reusability, and easy magnetic separation.

Hieu (2018) In this study, graphene oxide–manganese ferrite (GO–$MnFe_2O_4$) magnetic nanohybrids were synthesized via the co-precipitation technique and investigated for their adsorption properties in removing Cd(II) from contaminated water. The nanohybrids underwent thorough characterization using various techniques including X-ray diffraction, Fourier transform infrared spectroscopy, Brunauer–Emmett–Teller specific surface area analysis, transmission electron microscopy, and vibrating sample magnetometry.The characterization revealed high saturation magnetization values (Ms = 27.1 emu/g) and a specific surface area of 84.236 m2/g for the GO–$MnFe_2O_4$ nanohybrids. Adsorption experiments were conducted to evaluate the adsorption capacity of the nanohybrids and compared with MnFe2O4 nanoparticles and GO nanosheets.The equilibrium time for Cd(II) adsorption onto the nanohybrids was found to be 240 minutes. The experimental adsorption data fitted well with the Langmuir isotherm and the pseudo-second-order kinetic equation. Results indicated that the adsorption of Cd(II) using GO–$MnFe_2O_4$ magnetic nanohybrids outperformed $MnFe_2O_4$ and GO individually, with a maximum adsorption capacity of 121.951 mg/g at pH 8.

Molla et al. (2019)In this study, the adsorption behaviors of methylene blue (MB), rhodamine B (RhB), and methyl orange (MO) over graphene oxide (GO) were investigated experimentally and theoretically. Experimental results and characterizations of fresh GO and GO after adsorption revealed selective adsorption of positive dye molecules via electrostatic interactions between the =N+H group (positive dipole from dye molecules) and oxygen functional group of GO (negative dipole), as confirmed by zeta potential, FT-IR, and XPS analyses. The selectivity for positive dyes was rapid and quantitative, with removal efficiencies of 97% for MB and 88% for RhB achieved within 15 minutes, while the negative dye MO was not adsorbed. Ab initio molecular dynamics were employed to evaluate the most probable arrangement of dyes on GO and calculate the adsorption energy. The results indicated that MB exhibited stronger adsorption (-2.25 eV/molecule) on the GO surface compared to MO (-1.45 eV/molecule). The most favorable adsorption configuration occurred at 2,298 fs for MO and 2,290 fs for MB. Overall, this study highlights the selective adsorption capability of GO for positive dyes and provides insights into the underlying mechanisms through experimental and theoretical approaches.

Rani et al. (2017) This research focuses on the development of reduced graphene oxide/zinc ferrite (rGO/$ZnFe_2O_4$) nanocomposites for the photo-oxidative degradation of methylene blue (MB) dye. The nanocomposites were synthesized using a one-step solvothermal strategy, achieving simultaneous reduction of graphene oxide (GO) and Zn2+ and Fe3+ ions. Morphological studies revealed densely covered rGO sheets with 280-nm-sized spherical $ZnFe_2O_4$ nanostructures, with individual nanoparticles averaging 10 nm in size. The cubic spinel structure of the $ZnFe_2O_4$ nano-

materials was confirmed through diffraction patterns, and FT-IR spectroscopy was utilized to explore the nucleation sites for composite formation. The catalytic efficiency of the nanostructures for MB dye degradation in the presence of H2O2 was extensively evaluated, demonstrating remarkable catalytic activity of the rGO/$ZnFe_2O_4$ composite. The complete degradation of MB observed with the rGO/$ZnFe_2O_4$ composite is attributed to various interactions such as p–p interaction, hydrogen bonding, and electrostatic interaction between the composite and MB dye.

Chapter 3

Method of Preparation

The different routes available to synthesize spinel ferrites are solid state, co-precipitation, sol-gel, hydrothermal, microemulsion, solvothermal, etc.

The **Solid-state reaction method** for spinel ferrite formation involves a diffusion couple mechanism, typically using iron and metal salts. This process includes several steps like preparing the composition mixture, pre-sintering, powder conversion, and sintering. However, it has challenges such as uncontrolled stoichiometry, poor composition, and contamination. Wet chemical methods have become a preferred alternative, providing ferrite nanoparticles with reproducible composition and desired microstructures, overcoming many of the drawbacks of the solid-state approach.SOUFI et al. (2021)

Co-precipitation stands out as one of the oldest yet highly efficient methods for synthesizing spinel ferrites. It's valued for its convenience, cost effectiveness, and ability to produce large quantities rapidly while ensuring uniform particle size. The process involves adding stoichiometric amounts of metal salt solution into an alkaline solution with continuous stirring, where the pH plays a crucial role in determining the ferrite spinel type. Various SFs, including $CuFe_2O_4$, $CoFe_2O_4$, $MnFe_2O_4$, and $MgFe_2O_4$, have been successfully synthesized using this method. Monitoring and controlling the pH during the process are essential for achieving high-quality materials.SOUFI et al. (2021)

The **Sol-gel process** is a versatile method for synthesizing nano-ferrites and their composites, involving the transformation of liquid precursors into a colloidal solution (sol) and then into a network structure (gel). This approach is rapid, cost-effective, and yields highly pure and crystalline materials with uniform size distribution. Various terms like sol-gel auto-combustion, sol-gel autoignition, or gel-thermal decomposition describe different aspects of this process. Stoichiometric metal precursors are dissolved in water, and an organic fuel is added to adjust the pH and

promote gel formation, followed by evaporation and combustion to produce solid powder. Citric acid is commonly used due to its effectiveness as a complexing agent. The quality of the powder depends on factors like the nature of the fuel, precursors' concentration, pH, and annealing temperature. Numerous SFs, including $MgFe_2O_4$, $CuFe_2O_4$, $ZnFe_2O_4$, $NiFe_2O_4$, $CaFe_2O_4$, $CoFe_2O_4$, and $MnFe_2O_4$, have been successfully synthesized using this technique.SOUFI et al. (2021)

Microemulsion methods offer a thermodynamically stable system composed of two immiscible liquids and a surfactant, yielding nanoparticles with narrow size distribution and controllable size. This method, utilizing water, oil, and surfactant, allows precise control over particle properties such as size, morphology, and surface area. It can be categorized into oil-in-water (o/w) and water-in-oil (w/o) methods, both requiring surfactants above the critical micelle concentration (CMC). While eco-friendly and conducive to low-temperature synthesis with the possibility of surfactant reuse, drawbacks include poor crystallinity, solvent requirements, and polydispersion due to slower nucleation rates. Notably, spinel ferrites like $CoFe_2O_4$, $NiFe_2O_4$, $ZnFe_2O_4$, and Mn–Zn ferrite have been successfully synthesized using microemulsion methods.SOUFI et al. (2021)

Alternate routes available to synthesize Graphene oxide are Brodie method, Staudenmaier method, Hofmann's method, Hummer's method

Brodie method The first attempt to synthesize graphite oxide dates back to 1859 when British chemist B. C. Brodie conducted experiments on the reactivity of flake graphite. Brodie utilized a chlorate route, employing potassium chlorate as the oxidizing agent. He treated graphite with a mixture of potassium chlorate and fuming nitric acid at 60 °C for 4 days, resulting in what he termed as Brodie's graphene oxide (BR-GO). Subsequent oxidative treatments yielded a composition of carbon, oxygen, and hydrogen estimated as C11H4O5, corresponding to a C/O ratio of 2.2. Brodie's product, soluble in pure water but prone to flocculation in acidic environments, was named "graphic acid." JiÅ™Ã ÄkovÃ¡ et al. (2022)

The **Staudenmaier method**, another chlorate route, was later developed by L. Staudenmaier, who modified Brodie's approach by adjusting the addition of chlorate and incorporating sulfuric acid into the mixture, yielding Staudenmaier's graphene oxide (ST-GO). Potassium chlorate was added incrementally to mitigate the risk of explosive by-products, and the increased acidity reduced reaction times. The resulting material exhibited properties similar to BR-GO. JiÅ™Ã ÄkovÃ¡ et al. (2022)

Hofmann method In 1937, Hofmann synthesized Hofmann's graphene oxide (HO-GO) using potassium chlorate and nonfuming nitric acid, achieving a lower oxygen content (C/O ratio of 2.5). The concentration of nitric acid was found to significantly influence the oxidation level of the resulting graphene oxide.JiÅ™Ã ÄkovÃ¡ et al. (2022)

The **Hummer's method**, developed by Hummers and Offeman, emerged as the most widely used and effective approach. This method involves the reaction of graphite with an excess of potassium permanganate, sulfuric acid, and a small quantity of sodium nitrate, followed by neutralization with a diluted solution of hydrogen peroxide. The resulting product, Hummers' graphene oxide (HU-GO), shares a similar C/O ratio (2.25) with BR-GO but produces emissions during the reaction, rendering it environmentally unfriendly. Modified Hummers methods, including nitrate-free, two-step, co-oxidant, and low- and room-temperature variations, have been developed to address environmental concerns. JiÅ™Ã ÄkovÃ¡ et al. (2022)

3.1 Synthesis of Zinc Cobalt ferrite through Hydrothermal method.

Figure 3.1: Synthesis of Zinc Cobalt ferrite through Hydrothermal method

Three different samples ie.

- $Zn_{0.2}Co_{0.8}Fe_2O_4$
- $Zn_{0.5}Co_{0.5}Fe_2O_4$
- $Zn_{0.8}Co_{0.2}Fe_2O_4$

were prepared via hydrothermal route. Different metal salts such as Zinc acetate, Cobalt nitrate, Ferric nitrate were weighed along with CTAB. An aqueous solution of NaOH was prepared by dissolving 10 g of NaOH in 100 ml of distilled water. All the precursors where measured in stoichiometric ratios according to the the required concentration. CTAB was weighed according to the sum of the weight of zinc acetate, cobalt nitrate and ferric nitratenitrate. After weighing all

the precursors were added to 400 ml beaker containing distilled water. This solution was heated and stirred continuously for 1 hour. The freshly prepared aq. NaOH was added to the mixture to attain a basic pH. This mixture was then transferred to an autoclave and kept in oven for 24 hours at 180°C. After 24 hours the mixture was filtered and washed with HCl and distilled water. After this it was filtered with ethanol. The filtered samples were kept in oven at 90°C for drying. Then the samples were scrapped off of the filter paper, crushed and grinded to fine powder to yield the final zinc cobalt ferrite nanoparticles. Wang et al. (2013)

3.2 Synthesis of Graphene oxide through Modified Hummer's method.

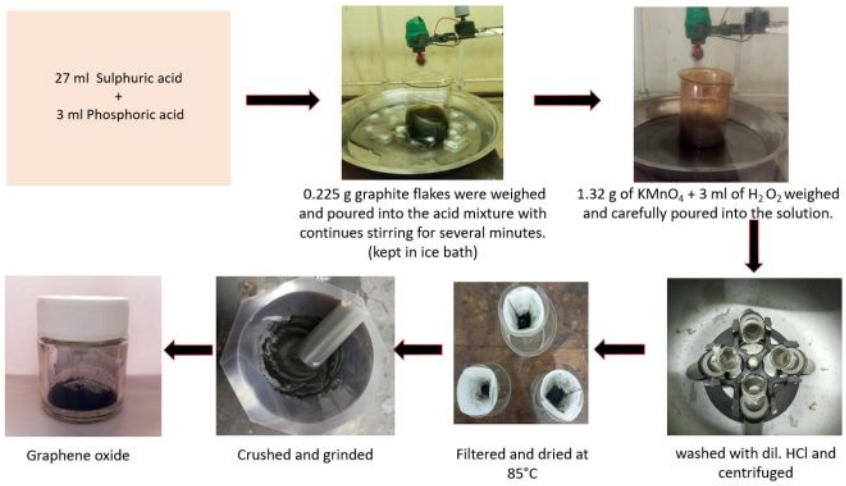

Figure 3.2: Synthesis of Graphene oxide through Modified Hummer's method

For synthesizing Graphene oxide, 27 ml of sulphuric acid and 3 ml of Phosphoric acid (volume ratio 9:1) were measurred and mixed together in a beaker and stirred. After this graphite flakes of 0.225 g were weighed and poured into the acid mixture with continues stirring for several minutes. Then 1.32 g of Potassium permanganate was weighed and carefully poured into the solution. This mixture was kept for stirring till the solution became dark green. Next, 3 ml of hydrogen peroxide was added slowly to the mixture to eliminate the excess of KMnO4 and stirred for 10 minutes. The reaction occurring being exothermic in nature, the reaction container (beaker) was kept in ice bath. Dilute HCl was added to the solution, and the solution was centrifuged at 700 rpm for 10 minutes, the supernatant was decanted and the residuals were rewashed with dil. HCl . These residuals were dried in oven at 85°C to yield the final Graphene oxide powder.Pushprajsinh H Rana (2021)

3.3 Synthesis of Zinc Cobalt ferrite Graphene oxide through Hydrothermal method.

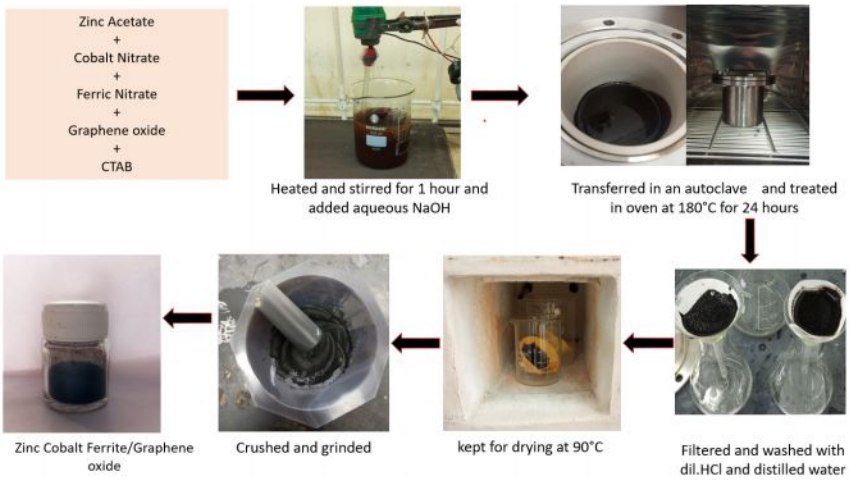

Figure 3.3: Synthesis of Zinc Cobalt ferrite Graphene oxide through Modified Hummer's method

Three different samples ie.

- $Zn_{0.2}Co_{0.8}Fe_2O_4$-GO
- $Zn_{0.5}Co_{0.5}Fe_2O_4$-GO
- $Zn_{0.8}Co_{0.2}Fe_2O_4$-GO

were prepared via hydrothermal route. Different metal salts such as Zinc acetate, Cobalt nitrate, Ferric nitrate were weighed along with Graphene oxide and CTAB. An aqueous solution of NaOH was prepared by dissolving 10 g of NaOH in 100 ml of distilled water. All the precursors where measured in stoichiometric ratios according to the the required concentration. CTAB was weighed according to the sum of the weight of zinc acetate, cobalt nitrate and ferric nitrate and Graphene oxide. After weighing all the precursors were added to 400 ml beaker containing distilled water. This solution was heated and stirred continuously for 1 hour. The freshly prepared aq. NaOH was added to the mixture to attain a basic pH. This mixture was then transferred to an autoclave and kept in oven for 24 hours at 180°C. After 24 hours the mixture was filtered and washed with HCl and distilled water. After this it was filtered with ethanol. The filtered samples were kept in oven at 90°C for drying. Then the samples were scrapped off of the filter paper, crushed and grinded to fine powder to yield the final zinc cobalt ferrite Graphene oxide nanocomposite. Verma et al. (2020)

Chapter 4

Characterization Techniques

4.1 X-Ray diffraction (XRD)

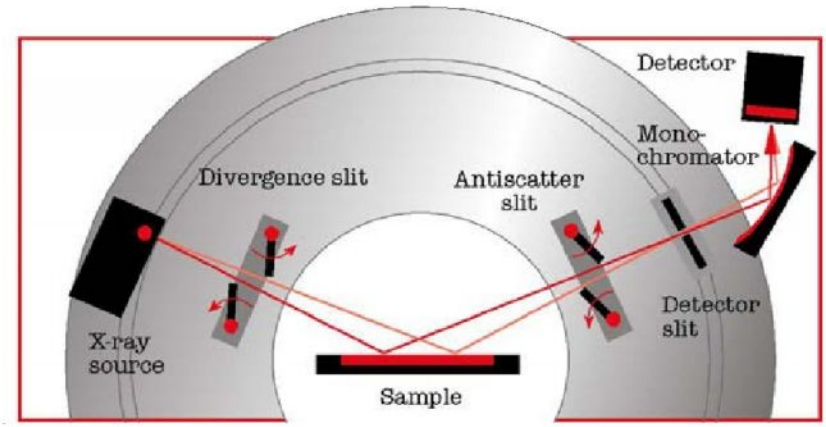

Figure 4.1: Schematic diagram of X-ray diffraction
Raman Venkatesan (2022)

X-ray diffraction is a highly effective nondestructive method used for characterizing crystalline materials. It offers insights into various structural aspects such as structures, phases, preferred crystal orientations (texture), and other parameters including average grain size, crystallinity, strain, and crystal defects. X-ray diffraction peaks result from the constructive interference of a monochromatic X-ray beam scattered at specific angles from each set of lattice planes within a sample. The intensities of these peaks are determined by the distribution of atoms within the

lattice, making the X-ray diffraction pattern a unique fingerprint of the periodic atomic arrangements in the material. Max von Laue and his colleagues made a significant discovery in 1912 when they found that crystalline substances act as three-dimensional diffraction gratings for X-ray wavelengths similar to the spacing of planes in a crystal lattice. This discovery laid the foundation for X-ray diffraction (XRD), which has since become a common technique for studying crystal structures and atomic spacing. X-ray diffraction relies on the constructive interference of monochromatic X-rays and a crystalline sample. X-rays are generated using a cathode ray tube, filtered to produce monochromatic radiation, collimated, and directed towards the sample. When the incident X-rays interact with the sample, they produce constructive interference, resulting in diffracted rays, following Bragg's law.

Figure 4.2: X-ray diffraction setup

X-ray diffractometers typically consist of three main components: an X-ray tube, a sample holder, and an X-ray detector. X-rays are generated in a cathode ray tube by bombarding a target material with accelerated electrons. The emitted X-rays, typically consisting of Ka and Kb components, are filtered to produce monochromatic radiation before being directed onto the sample. The diffracted X-rays are collected by a detector, and the intensity is recorded as the sample is rotated. The geometry of an X-ray diffractometer involves rotating the sample at an angle u while the detector collects diffracted X-rays at an angle of 2u. This setup allows for the collection of data across a range of angles, typically from 5° to 70°, during the X-ray scan. X-ray powder diffraction is widely used for identifying unknown crystalline materials, such as minerals and inorganic compounds, with applications in various fields including geology, environmental science, material science, engineering, and biology. XRD can also be utilized for determining crystal

structures, quantifying mineral amounts, characterizing thin film samples, and making textural measurements in polycrystalline samples. Specialized techniques, such as Rietveld refinement, enable more advanced analysis of crystal structures and properties.

Sample Preparation: Proper sample preparation is crucial for accurate analysis of powder samples using X-ray diffraction , particularly for materials like soils, clays, and other substances with complex compositions. These materials often contain finely divided colloids, iron oxide coatings, and organic matter, which can interfere with XRD analysis.

Sample preparation involves not only removing undesirable substances but also employing techniques to control particle size, orientation, thickness, and other parameters. For XRD analysis of powders, it's essential that they are finely ground to achieve a good signal-to-noise ratio, avoid spottiness, and minimize preferred orientation. The recommended particle size range is typically around 1–5 micrometer. There are two common types of mounts used for XRD analysis, depending on the desired crystallite orientation. Random mounts are preferred for phase identification, where particles are ground to 1–5 micrometer and packed onto a flat surface in various orientations to ensure reflections from different crystal planes (hkl).

Oriented mounts are used when analyzing clay minerals, which often exhibit strong diffraction effects primarily from specific crystal planes, such as (001). For these samples, a slurry of the material with distilled water is prepared, and the water is allowed to evaporate until the sample is smeared onto a sample holder, such as a glass slide or ceramic tile. This process helps ensure a consistent orientation of the crystalline particles for more accurate XRD analysis. Andrei A. Bunaciu and Aboul-Enein (2015)

4.2 UV-Vis spectroscopy

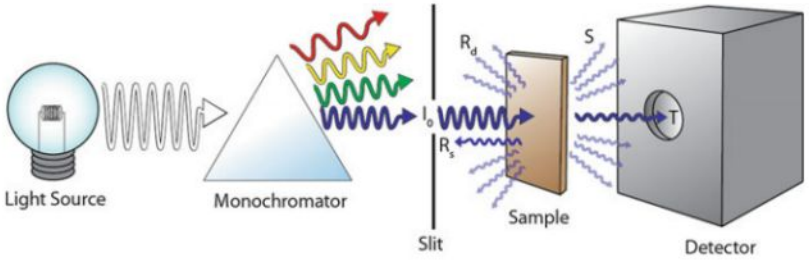

Figure 4.3: Schematic diagram of UV-Vis Spectroscopy
Chen et al. (2013)

UV-Vis spectroscopy provides valuable insights into electronic transitions within materials by

measuring light absorption as a function of wavelength. The Beer-Lambert law describes the relationship between the fraction of light transmitted through a sample and its absorption properties. This law, often simplified as Beer's Law, relates the absorbance (A) to the concentration of the absorbing species, the path length of light through the sample, and the molar absorptivity coefficient.

$$A = \varepsilon c l = -\log_{10}\left(\frac{I}{I_0}\right)$$

Where: - A is the absorbance - ε is the molar absorptivity coefficient - c is the concentration of the absorbing species - l is the path length of light through the sample - I is the intensity of the light transmitted through the sample - I_0 is the incident intensity of the light

The absorbance can be further normalized to the path length, yielding the absorption coefficient (α), which is commonly used for characterizing semiconductors and estimating the optical band gap.

$$\alpha = \frac{\ln 10 \times A}{l}$$

UV-Vis spectroscopy is particularly useful for estimating the optical band gap of semiconductors by probing electronic transitions between the valence and conduction bands. This gap may differ from the electronic band gap, which is the energy difference between the valence band maximum and the conduction band minimum. UV-Vis spectroscopy can also provide insights into the nature of electronic transitions (direct or indirect) and their selection rules.

Overall, UV-Vis spectroscopy offers valuable information about electronic transitions in materials, although interpretation can be complex due to factors such as exciton binding energies, phonon absorptions, and dipole selection rules. Nonetheless, it remains a powerful tool for characterizing the optical properties of materials. Chen et al. (2013)

4.3 Raman Spectroscopy

Raman spectroscopy is a technique used to analyze the intensity and wavelength of light scattered from molecules or crystals. It is applicable to both organic and inorganic samples. In Raman spectroscopy, a sample is exposed to light of known polarization and wavelength, typically in the visible or infrared ranges. Inelastic scattering, known as Raman scattering, occurs, resulting in a wavelength-shifted spectrum compared to the incident light.

The Raman spectrum provides information about molecular vibrations or phonons in a crys-

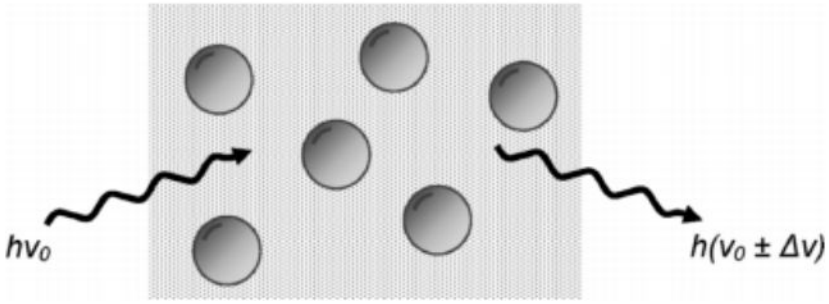

Figure 4.4: Schematic diagram Raman scattering
Kalantar-zadeh and Fry (2008)

tal. By analyzing the wavenumbers of Raman shifts against their respective intensities, valuable insights into molecular structure and composition can be obtained. This technique is often used for qualitative and quantitative analysis of materials.

In sensing applications, Raman spectroscopy can provide quantitative information about analyte molecules and their interactions. Changes in peak intensities and positions can indicate variations in the number of bonds or functional groups within molecules.

Raman scattering can result in either Stokes emission (lower energy) or anti-Stokes emission (higher energy), depending on whether the scattered photon gains or loses energy compared to the incident light. Although there is a change in wavelength, no energy is lost during the interaction. The shift in intensity and frequency is determined by the polarizability of the electron cloud in a bond.

Despite its utility, Raman scattering comprises only a small fraction of the scattered light, making it challenging to discern weak Raman signals from intense Rayleigh scattered light. Photoluminescence, which can obscure the Raman spectrum, may also occur depending on the incident light energy. However, anti-Stokes shifts are less susceptible to photoluminescence interference.

Surface Enhanced Raman Spectroscopy (SERS) is a technique used to enhance Raman signals by adsorbing molecules onto roughened metal surfaces, typically gold or silver. This method exploits changes in analyte polarizability perpendicular to the surface, resulting in significant signal enhancement. Kalantar-zadeh and Fry (2008)

4.4 Scanning Electron Microscopy (SEM)

Scanning Electron Microscopy (SEM) is a widely used technique for characterizing nanomaterials, offering nanoscale resolution in imaging and providing valuable insights into the topography and morphology of materials. In an SEM, secondary electron images are obtained by scanning an elec-

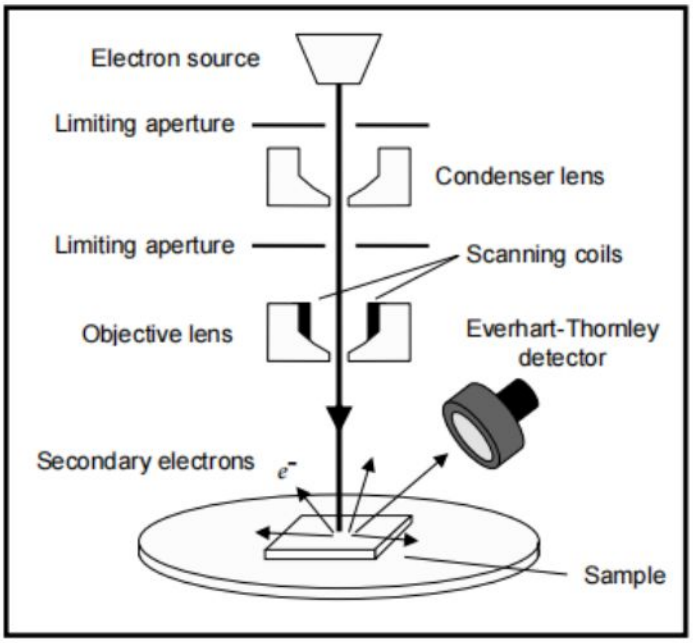

Figure 4.5: Schematic diagram of Scanning Electron Microscopy
Kalantar-zadeh and Fry (2008)

tron probe across a sample surface and monitoring the secondary electrons emitted. Additionally, compositional analysis can be performed by detecting X-rays produced by the electron-specimen interaction, allowing detailed elemental distribution maps to be generated. The electron beam in

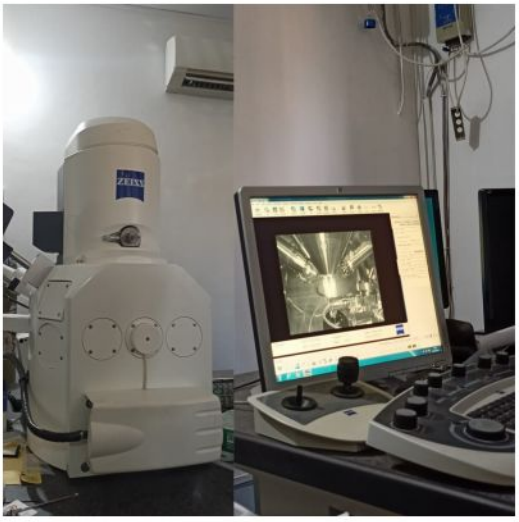

Figure 4.6: Scanning Electron Microscopy setup

an SEM is emitted from a heated filament, typically made from lanthanum hexaboride (LaB6) or tungsten. Alternatively, electrons can be emitted via field emission (FE). These electrons are accelerated towards the sample by applying an electric potential and then focused and raster-scanned

over the sample surface by scanning coils. When the primary electrons strike the sample, they transfer energy to the sample electrons, resulting in the emission of secondary electrons. These secondary electrons are collected by a detector, converted to a voltage, amplified, and used to build an image displaying intensity versus the position of the primary beam on the sample. Sam-

ples placed in an SEM must either be conducting or covered with a thin metal layer to avoid electric charging. Scanning typically occurs at low pressures to prevent electron scattering by gas molecules inside the chamber. SEM allows imaging of comparatively large areas of the sample and can also detect high-energy electrons backscattered from the specimen interaction volume, providing contrast between areas with different chemical compositions.

In nanotechnology and sensing applications, SEM plays a crucial role in understanding the interaction between sensing layers and analytes. Surface morphology and topography strongly influence sensitivity, and SEM imaging helps researchers optimize sensor performance. SEM can monitor the formation and growth of thin films, nanostructures, and nanorods, providing detailed insights into their characteristics. Additionally, SEM can study multilayered materials and nanostructures by examining their cross sections, allowing observation of their conformation to substrates and the thickness of each layer. All information obtained from SEM imaging can be correlated with sensor response, aiding in sensor optimization. Kalantar-zadeh and Fry (2008)

4.5 Dielectric measurement

Dielectric spectroscopy (DS), also known as impedance spectroscopy or electrochemical impedance spectroscopy, is a valuable technique used to study the response of a sample to an applied electric field of either fixed or varying frequency. DS provides insights into the dielectric properties of

materials as a function of frequency, making it a powerful tool for investigating molecular dynamics and material parameters like static dielectric permittivity () and DC electrical conductivity ().

The principle behind DS involves the interaction of applied alternating electric fields with dipoles possessing reorientation mobility in materials. By measuring the response of the material to the applied electric field, DS can determine the frequency-dependent complex permittivity, which includes information about the dielectric constant (0), dielectric loss (tan), and other related parameters.

DS is widely used in the study of soft matter, polymers, polymer nanocomposites, and nanomaterials. It operates across a broad frequency range, from very low frequencies (mHz) suitable for analyzing interfaces between insulation components to very high frequencies (THz).

In summary, DS provides valuable insights into the dielectric properties of materials across a wide frequency range, making it a versatile and powerful technique for studying molecular dynamics and material characteristics. Deshmukh et al. (2017)

The dielectric properties of materials play a crucial role in various applications, ranging from electronics to materials science and beyond. These properties are determined by how the material responds to an electric field, particularly in terms of polarization.

Dielectrics support charge by undergoing polarization when subjected to an electric field. This polarization results in the development of a net positive charge on one surface and a net negative charge on the opposite surface. This phenomenon occurs due to the alignment or reorientation of electric dipoles within the material.

All non-conducting materials, including insulators, exhibit electronic polarization to some degree. This means that they can support charge through the movement or alignment of electrons within the material. In contrast, materials with ions or permanent dipoles can exhibit additional types of polarization, such as ionic polarization or dipole polarization, respectively.

Accurately measuring the dielectric properties of materials provides valuable information for incorporating them into various applications. For example, in electronics, understanding the dielectric properties of insulating materials is essential for designing capacitors, transformers, and other electronic components. In materials science, monitoring dielectric properties during manufacturing processes helps ensure the quality and performance of the final product. The dielectric constant, is a fundamental property of a material that quantifies its ability to store electrical energy in an electric field. It indicates how much electric flux the material can hold or concentrate relative to a vacuum or free space. Van Uitert (1956) Kuru et al. (2020)

Chapter 5

Results and Discussion

5.1 X-Ray Diffraction (XRD)

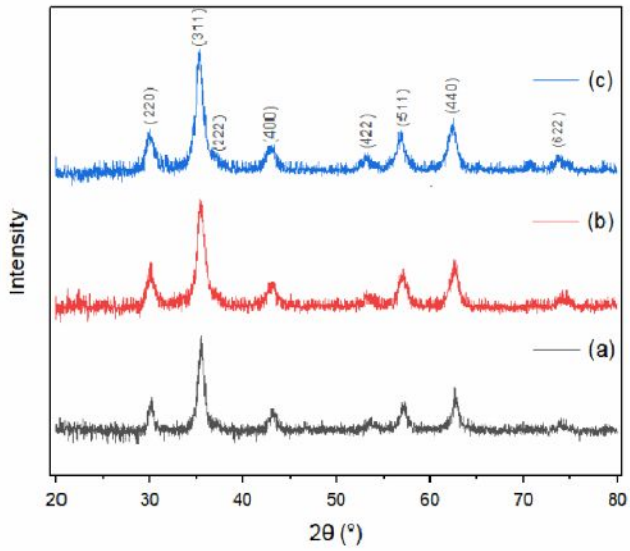

Figure 5.1: XRD pattern of (a) $Zn_{0.2}Co_{0.8}Fe_2O_4$, (b) $Zn_{0.5}Co_{0.5}Fe_2O_4$, (c) $Zn_{0.8}Co_{0.2}Fe_2O_4$

The X-Ray diffraction patterns of $Zn_xCo_{1-x}Fe_2O_4$ and $Zn_xCo_{1-x}Fe_2O_4$/GO are shown in the fig.5.1 and 5.3 respectively. The prominent Bragg reflections were seen a 2θ values of 18.3, 30.1, 35.4, 36.9, 43.1, 53.5, 57.0, 62.6, 74.1 indexed as (111), (220), (311), (222), (400), (422), (511), (440), (533) respectively , which indicated the formation of the cubic spinel phase having space group Fd3m.Meidanchi and Ansari (2021)

Figure 5.2 shows Graphene oxide diffraction peaks at 10 indexed as (001). Graphene oxide being derived from Graphite, which usually shows peak at 26, is seen to be absent, which indicates

that it is completely oxidized and Graphene oxide is formed. Handayani et al. (2019)

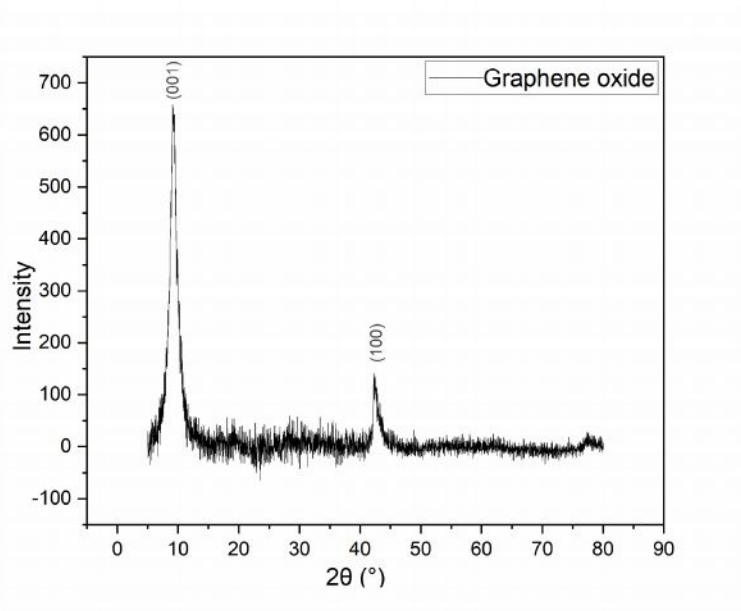

Figure 5.2: XRD pattern of Graphene oxide.

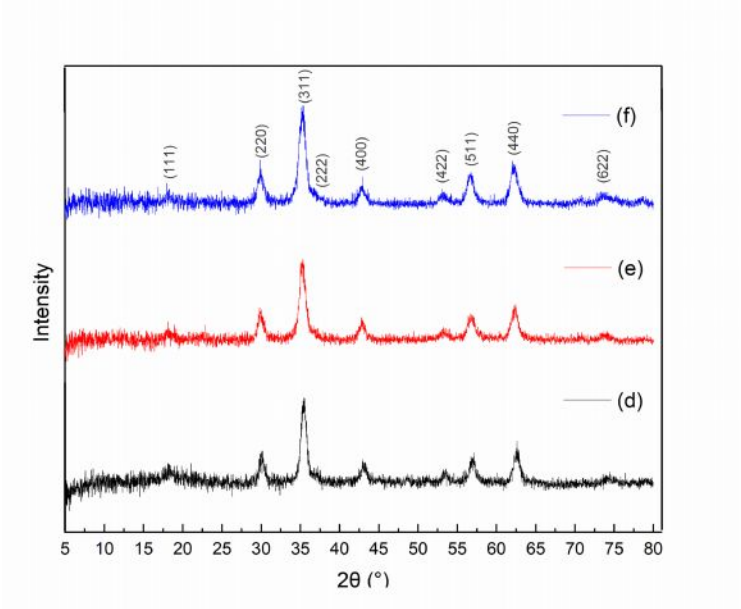

Figure 5.3: XRD pattern of (d) $Zn_{0.2}Co_{0.8}Fe_2O_4$/GO (e) $Zn_{0.5}Co_{0.5}Fe_2O_4$/GO (f) $Zn_{0.8}Co_{0.2}Fe_2O_4$/GO

The absence of a Graphene oxide diffraction peak in the ferrite/GO nanocomposite shown in the figure 5.3, suggests that the regular layered structure of GO has been disrupted due to the crystal growth occuring between the interlayers of GO. Bayantong et al. (2021a)

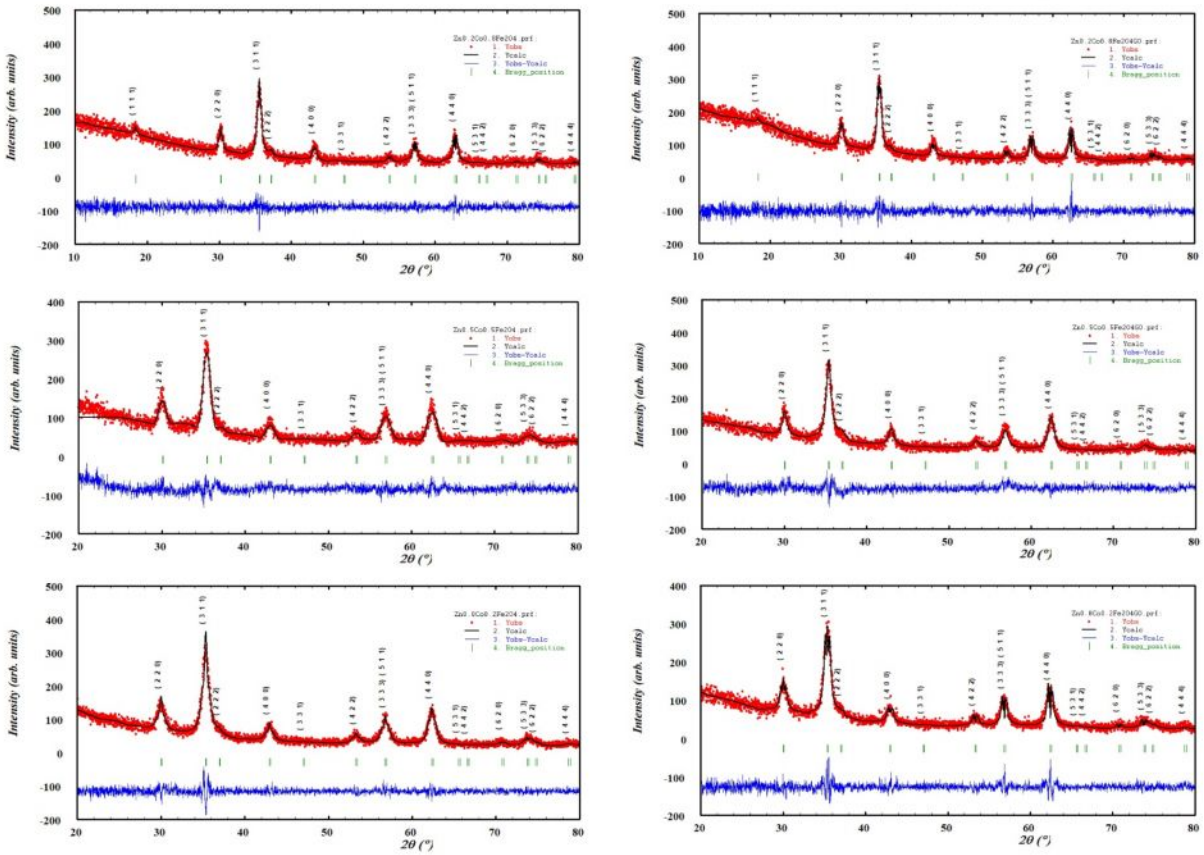

Figure 5.4: Rietveld refinement of (a) $Zn_{0.2}Co_{0.8}Fe_2O_4$, (b) $Zn_{0.5}Co_{0.5}Fe_2O_4$, (c) $Zn_{0.8}Co_{0.2}Fe_2O_4$ and (d) $Zn_{0.2}Co_{0.8}Fe_2O_4$/GO(7.5%) , (e) $Zn_{0.5}Co_{0.5}Fe_2O_4$/GO(7.5%) , (f) $Zn_{0.8}Co_{0.2}Fe_2O_4$/GO(7.5%)

Further, the variations of Lattice constant 'a', Crystallite size 't', Strain, were studied with increasing Co^{2+} concentration as shown in figure 5.5

Figure 5.5 shows the variation of lattice constant with Cobalt concentration. The lattice constant is seen to decrease with increase in Cobalt concentration,which can be attributed to smaller ionic radii of cobalt as compared to that of Zinc. The crystallite size is seen to increase with increasing cobalt concentration. Further, This may be attributed to the reduction in lattice strain which could be because of the inclusion of a smaller ion (as cobalt concentration increases) in the ferrite structure that causes lattice to grow to the larger dimensions causing the crystallite size to increase. Naik et al. (2020)

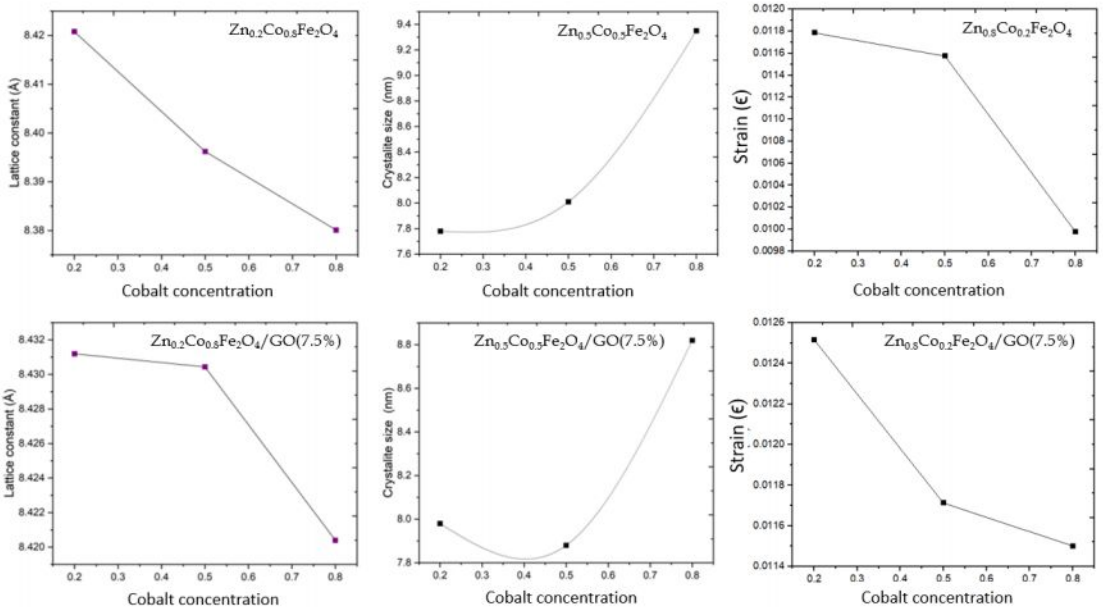

Figure 5.5: Variations of Lattice constant 'a' and Crystallite size 't' and Strain 'ϵ' with increasing Cobalt concentration

5.2 Raman Spectroscopy

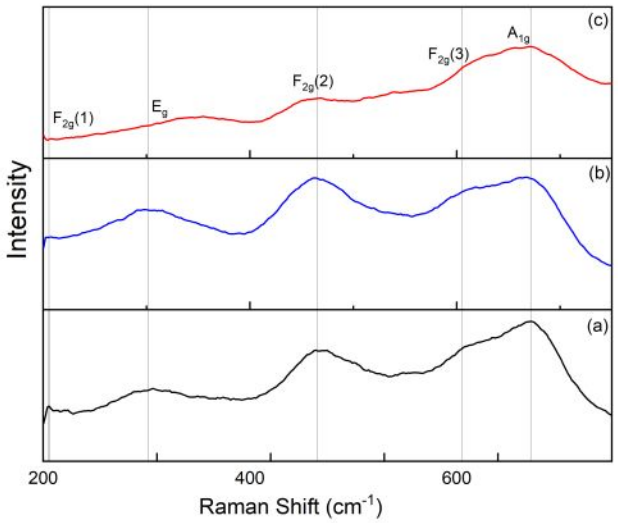

Figure 5.6: Raman Spectra of (a) $Zn_{0.2}Co_{0.8}Fe_2O_4$, (b) $Zn_{0.5}Co_{0.5}Fe_2O_4$, (c) $Zn_{0.8}Co_{0.2}Fe_2O_4$

Figure 5.6 shows Raman spectra of $ZnCoFe_2O_4$ nanoparticles which showed distinctive peaks at 205 cm^{-1}, 302 cm^{-1}, 464 cm^{-1}, 604 cm^{-1}, 671 cm^{-1} which can be indexed as $F_{2g}(1)$, E_g, $F_{2g}(2)$, $F_{2g}(3)$, A_{1g} modes respectively. The 671 cm^{-1} mode corresponds to symmetric stretching and bending of oxygen in octahedral site is seen at 464 cm^{-1} and 604 cm^{-1} that is $F_{2g}(2)$ and $F_{2g}(3)$ respectively. The band at 205 cm^{-1} corresponds to $F_{2g}(1)$ mode, caused by the translation

movement of the whole tetrahedron. The two prominent peaks at 1346 cm^{-1} and 1590 cm^{-1} figure 5.8 indicate disordered carbon (D) and Ordered carbon (G) respectively. Rani et al. (2017)

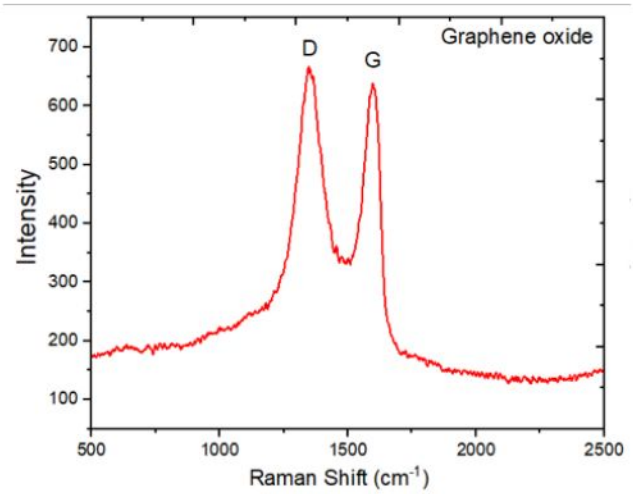

Figure 5.7: Raman Spectra of Graphene oxide

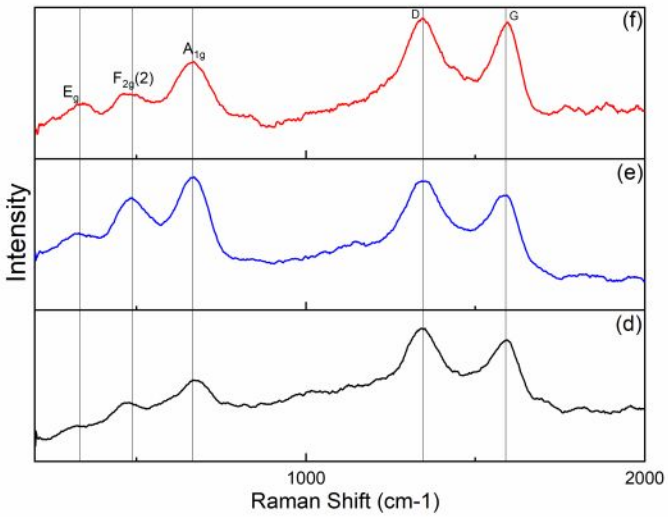

Figure 5.8: Raman Spectra of (d) $Zn_{0.2}Co_{0.8}Fe_2O_4$/GO(7.5%) (e) $Zn_{0.5}Co_{0.5}Fe_2O_4$/GO(7.5%) (f) $Zn_{0.8}Co_{0.2}Fe_2O_4$/GO(7.5%)

5.3 Scanning electron microscopy

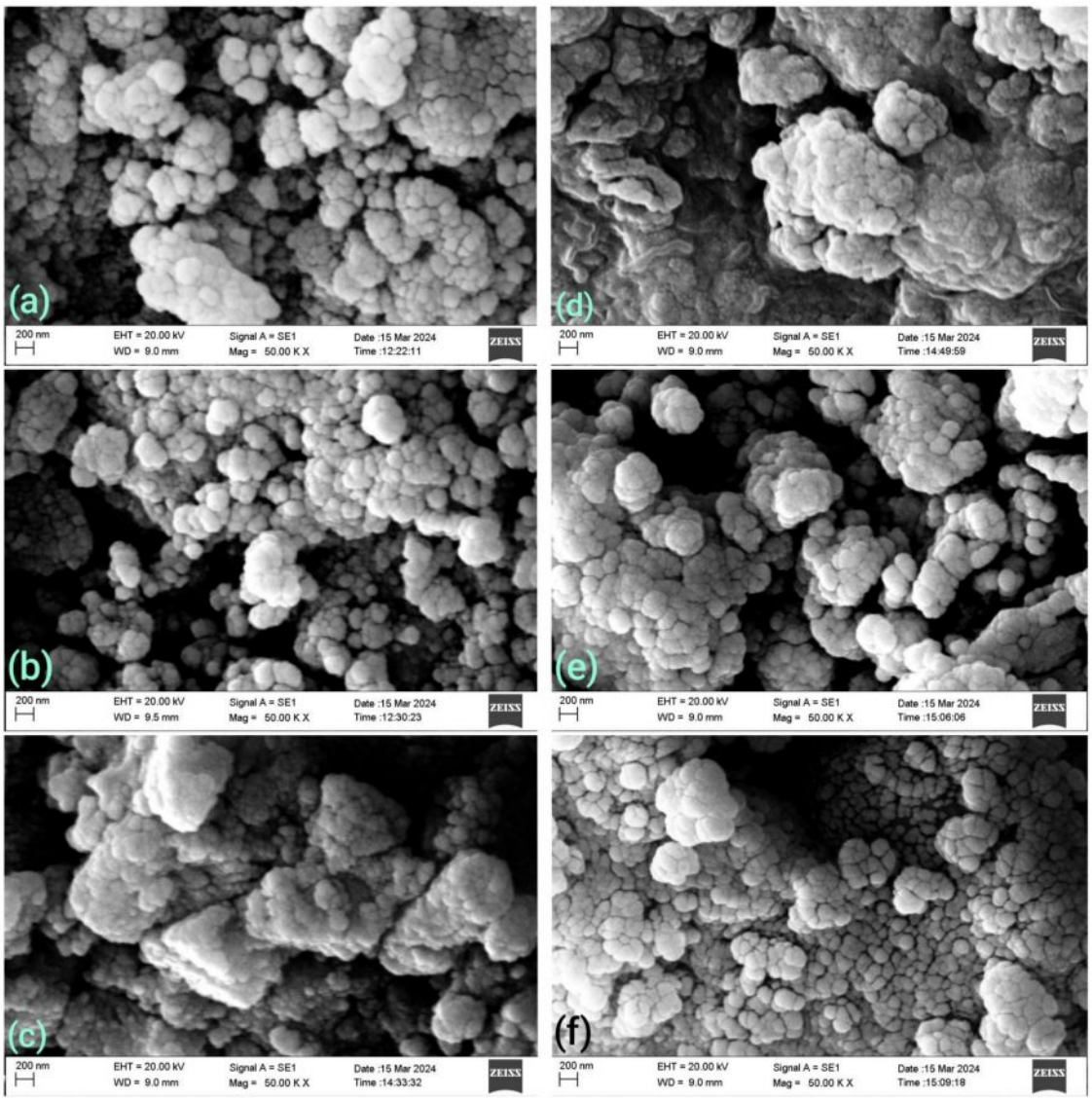

Figure 5.9: Scanning electron microscopy images of (a) $Zn_{0.2}Co_{0.8}Fe_2O_4$, (b) $Zn_{0.5}Co_{0.5}Fe_2O_4$, (c) $Zn_{0.8}Co_{0.2}Fe_2O_4$ (d) $Zn_{0.2}Co_{0.8}Fe_2O_4$/GO(7.5%) (e) $Zn_{0.5}Co_{0.5}Fe_2O_4$/GO(7.5%) (f) $Zn_{0.8}Co_{0.2}Fe_2O_4$/GO(7.5%)

The morphology of the prepared samples were studied using the Carl Zeiss Scanning Electron Microscope. The SEM images 5.9 of the prepared nanoparticles and nanocomposites showed the formation of quasi spherical nano range particles with aglomerations.

5.4 Dielectric Spectroscopy

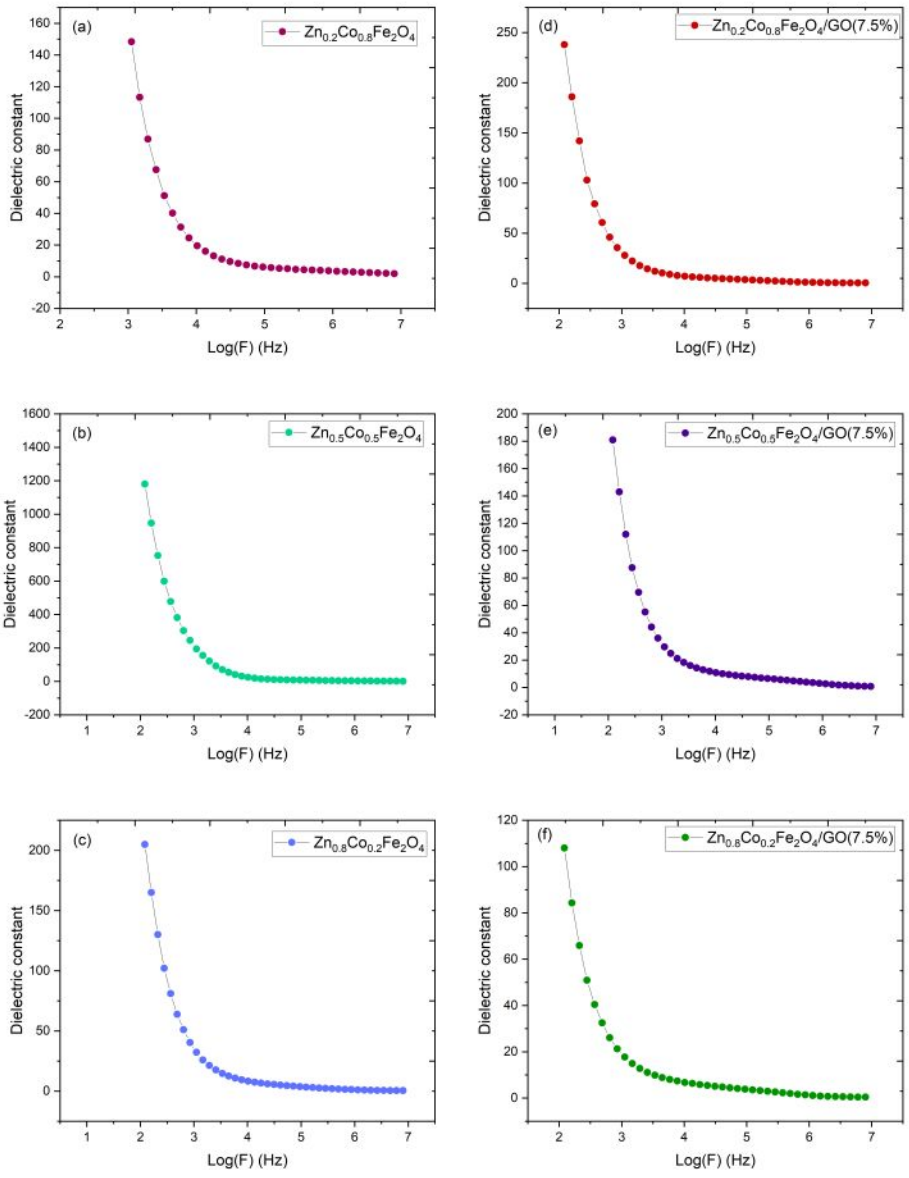

Figure 5.10: Dielectric constant as a function of frequency

The dielectric constant values of the samples are plotted as a function of frequency as shown in figure 5.10. The dielectric constant is seen to decrease with increase in frequency. The dielectric constant for lower frequencies was seen to be increasing as graphene oxide was incooperated with Zinc Cobalt ferrite nanoparticles, which could be attributed to the fact that graphene oxide is a better conductor than the ferrites, except for the $Zn_{0.2}Co_{0.8}Fe_2O_4$ and $Zn_{0.2}Co_{0.8}Fe_2O_4$/GO. Rani

et al. (2017)

5.5 Adsorption of Methylene blue dye

Adsorption is the adhesion of molecules of adsorbate onto the surface of adsorbent. During this process, the dye molecules are attracted to the surface of the adsorbent material, forming a thin film or a layer on its surface. This attraction occurs due to forces such as Van der Waals forces, electrostatic interactions, and hydrogen bonding between the dye molecules and the surface of the adsorbent. This interaction is influenced by factors such as surface area, pore size, and chemical properties of the adsorbent. Once the dye molecules are adsorbed onto the surface of the material, they are effectively removed from the solution, leading to the purification or separation of the dye from the medium. One of the key objectives of studying dye adsorption is to improve the efficiency of dye removal from wastewater, contributing to environmental sustainability. In this process the adsorbents are exposed to a solution of dye, allowing the dye molecules to interact with the material's surface. Next, the adsorption capacity of each adsorbent is analysed by measuring the concentration of dye remaining in the solution after adsorption has taken place. Weng and Pan (2007) Gürses et al. (2006)

For the dye adsorption experiment, dye solution of 5 ppm concentration was prepared. 10 ml of this solution was taken for tesing ,into which 50 mg of the prepared adsorbent was added. Afer 20 mins, adsorption to take place, the solution was centrifuged to separate the added adsorbent from the dye solution. Sadighian et al. (2018) Naik et al. (2020)

The obtained results are shown in the figure 5.11. Where in it is seen that the dye removal by the Zinc Cobalt ferrite nanoparticles is approximately 38% and dye removal by the Zinc Cobalt ferrite/ Graphene oxide nanocomposite is nearly 60%.

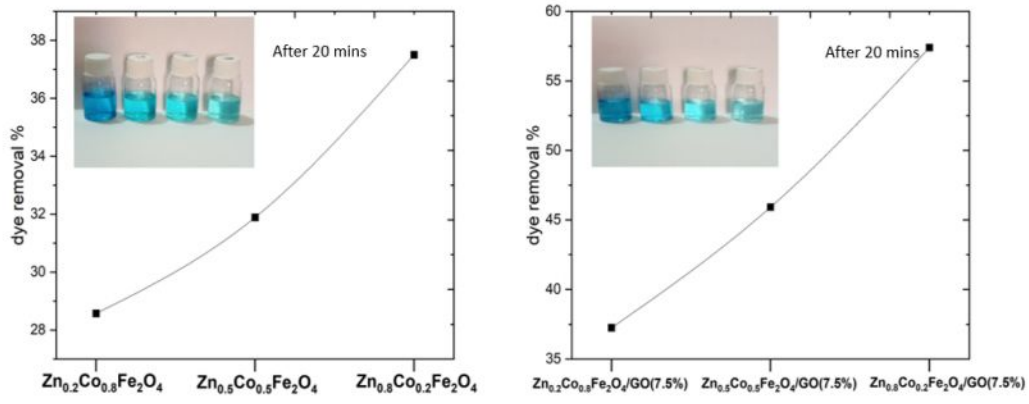

Figure 5.11: Adsorption of Methylene blue dye

Bibliography

Adel, M., Ahmed, M., and Mohamed, A. (2021). Effective removal of indigo carmine dye from wastewaters by adsorption onto mesoporous magnesium ferrite nanoparticles. *Environmental Nanotechnology, Monitoring and Management*, 16:100550.

Andrei A. Bunaciu, E. g. U. and Aboul-Enein, H. Y. (2015). X-ray diffraction: Instrumentation and applications. *Critical Reviews in Analytical Chemistry*, 45(4):289–299. PMID: 25831472.

Bayantong, Allen Rhay B., S., Yu-Jen, D., Cheng-Di, G.-S., and , Sergi de Luna, M. D. G. (2021a). Nickel ferrite nanoenabled graphene oxide (nife2o4go) as photoactive nanocomposites for water treatment. *Environmental Science and Pollution Research*.

Bayantong, A. R. B., Shih, Y.-J., Ong, D. C., Ababarca, R. R. M., Dong, C.-D., and de Luna, M. D. G. (2021b). Adsorptive removal of dye in wastewater by metal ferrite-enabled graphene oxide nanocomposites. *Chemosphere*, 274:129518.

Baynosa, M. L., Mady, A. H., Nguyen, V. Q., Kumar, D. R., Sayed, M. S., Tuma, D., and Shim, J.-J. (2020). Eco-friendly synthesis of recyclable mesoporous zinc ferrite@reduced graphene oxide nanocomposite for efficient photocatalytic dye degradation under solar radiation. *Journal of Colloid and Interface Science*, 561:459–469.

Chen, Z., Deutsch, T., Dinh, H., Domen, K., Emery, K., Forman, A. J., Gaillard, N., Garland, R., Heske, C., Jaramillo, T., Kleiman-Shwarsctein, A., Miller, E., Takanabe, K., and Turner, J. (2013). Uv-vis spectroscopy. pages 49–62.

Cwalinski, T., Polom, W., Marano, L., Roviello, G., D'Angelo, A., Cwalina, N., Matuszewski, M., Roviello, F., Jaskiewicz, J., and Polom, K. (2020). Methylene blue—current knowledge, fluorescent properties, and its future use. *Journal of Clinical Medicine*, 9.

Das, P., Debnath, P., and Debnath, A. (2021). Enhanced sono-assisted adsorptive uptake of malachite green dye onto magnesium ferrite nanoparticles: Kinetic, isotherm and cost analysis. *Environmental Nanotechnology, Monitoring and Management*, 16:100506.

Deshmukh, K., Sankaran, S., Ahamed, B., Sadasivuni, K. K., Pasha, K. S., Ponnamma, D., Rama Sreekanth, P., and Chidambaram, K. (2017). Chapter 10 - dielectric spectroscopy. In Thomas, S., Thomas, R., Zachariah, A. K., and Mishra, R. K., editors, *Spectroscopic Methods for Nanomaterials Characterization*, Micro and Nano Technologies, pages 237–299. Elsevier.

Dideikin, A. and Vul, A. (2019). Graphene oxide and derivatives: The place in graphene family. *Frontiers in Physics*.

Fobiri, G. (2022). Synthetic dye application in textiles: A review on the efficacies and toxicities involved. *Textile Leather Review*, 5:180–198.

Gerani, K., Mortaheb, H., and Mokhtarani, B. (2016). Enhancement in performance of sulfonated pes cation exchange membrane by introducing pristine and sulfonated graphene oxide nanosheets synthesized through hummers and staudenmaier methods. *Polymer-Plastics Technology and Engineering*, 56.

Ghobadi, M., Gharabaghi, M., Abdollahi, H., Boroumand, Z., and Moradian, M. (2018). Mnfe2o4-graphene oxide magnetic nanoparticles as a high-performance adsorbent for rare earth elements: Synthesis, isotherms, kinetics, thermodynamics and desorption. *Journal of Hazardous Materials*, 351:308–316.

Gürses, A., Doğar, , Yalcin, M., Açıkyıldız, M., Bayrak, R., and Karaca, S. (2006). The adsorption kinetics of the cationic dye, methylene blue, onto clay. *Journal of hazardous materials*, 131 1-3:217–28.

Handayani, M., Sulistiyono, E., Rokhmanto, F., Darsono, N., Fransisca, P. L., Erryani, A., and Wardono, J. T. (2019). Fabrication of graphene oxide/calcium carbonate/chitosan nanocomposite film with enhanced mechanical properties. *IOP Conference Series: Materials Science and Engineering*, 578(1):012073.

Hieu, N. H. (2018). Removal of cd(ii) from water by using graphene oxide–mnfe2o4 magnetic nanohybrids. *Vietnam Journal of Science and Technology*, 55:109.

JiÅ™Ã ÄkovÃ¡, A., JankovskÃ½, O., Sofer, Z., and SedmidubskÃ½, D. (2022). Synthesis and applications of graphene oxide. *Materials*, 15(3).

Jose Varghese, R., hadji Mamour Sakho, E., Parani, S., Thomas, S., Oluwafemi, O. S., and Wu, J. (2019). Chapter 3 - introduction to nanomaterials: synthesis and applications. In Thomas, S., Sakho, E. H. M., Kalarikkal, N., Oluwafemi, S. O., and Wu, J., editors, *Nanomaterials for Solar Cell Applications*, pages 75–95. Elsevier.

Kalantar-zadeh, K. and Fry, B. (2008). *Characterization Techniques for Nanomaterials*.

Katubi, K. M. M., Alsaiari, N. S., Alzahrani, F. M., M. Siddeeg, S., and A. Tahoon, M. (2021). Synthesis of manganese ferrite/graphene oxide magnetic nanocomposite for pollutants removal from water. *Processes*, 9(4).

Khan, I., Saeed, K., Zekker, I., Zhang, B., Hendi, A. H., Ahmad, A., Ahmad, S., Zada, N., Ahmad, H., Shah, L. A., Shah, T., and Khan, I. (2022). Review on methylene blue: Its properties, uses, toxicity and photodegradation. *Water*, 14(2).

Kuru, M., Kuru, T. , Karaca, E., and Bağcı, S. (2020). Dielectric, magnetic and humidity properties of mg–zn–cr ferrites. *Journal of Alloys and Compounds*, 836:155318.

Lan Huong, P. T., Tu, N., Lan, H., Thang, L. H., Van Quy, N., Tuan, P. A., Dinh, N. X., Phan, V. N., and Le, A.-T. (2018). Functional manganese ferrite/graphene oxide nanocomposites: effects of graphene oxide on the adsorption mechanisms of organic mb dye and inorganic as(v) ions from aqueous solution. *RSC Adv.*, 8:12376–12389.

López, J., Ortiz, A., Muñoz-Muñoz, F., Domínguez, D., León, J. N. D., Galindo, J., Hogan, T., Gomez, S., Tiznado, H., and Herrera, G. (2021). Magnetic nanostructured based on cobalt–zinc ferrites designed for photocatalytic dye degradation. *Journal of Physics and Chemistry of Solids*, 150:109869.

Mahmoodi, N. M. (2013). Zinc ferrite nanoparticle as a magnetic catalyst: Synthesis and dye degradation. *Materials Research Bulletin*, 48:4255–4260.

Mandal, B., Panda, J., Paul, P. K., Sarkar, R., and Tudu, B. (2020). Mnfe2o4 decorated reduced graphene oxide heterostructures: Nanophotocatalyst for methylene blue dye degradation. *Vacuum*, 173:109150.

Marcano, D., Kosynkin, D., Berlin, J., Sinitskii, A., Sun, Z., Slesarev, A., Alemany, L., Lu, W., and Tour, J. (2010). Improved synthesis of graphene oxide. *ACS nano*, 4 8:4806–14.

Meidanchi, A. and Ansari, H. (2021). Copper spinel ferrite superparamagnetic nanoparticles as a novel radiotherapy enhancer effect in cancer treatment. *Journal of Cluster Science*.

Molla, A., Li, Y., Mandal, B., Kang, S., Hur, S., and Chung, J. (2019). Selective adsorption of organic dyes on graphene oxide: Theoretical and experimental analysis. *Applied Surface Science*.

Naik, A. B., Naik, P. P., Hasolkar, S. S., and Naik, D. (2020). Structural, magnetic and electrical properties along with antifungal activity adsorption ability of cobalt doped manganese ferrite nanoparticles synthesized using combustion route. *Ceramics International*, 46(13):21046–21055.

Oladoye, P. O., Ajiboye, T. O., Omotola, E. O., and Oyewola, O. J. (2022). Methylene blue dye: Toxicity and potential elimination technology from wastewater. *Results in Engineering*, 16:100678.

Pacakova, B., Kubickova, S., Reznickova, A., Niznansky, D., and Vejpravova, J. (2017). Spinel ferrite nanoparticles: Correlation of structure and magnetism. In Seehra, M. S., editor, *Magnetic Spinels*, chapter 1. IntechOpen, Rijeka.

Pham, T. N., Huy, T. Q., and Le, A.-T. (2020). Spinel ferrite (afe2o4)-based heterostructured designs for lithium-ion battery, environmental monitoring, and biomedical applications. *RSC Adv.*, 10:31622–31661.

Pushprajsinh H Rana, M. M. (2021). Preparation of graphene oxidefrom graphite powder using hummer's modified method. *International journal of creative research thoughts.*

Ramachandran Ph.D, T. and Vishista, k. (2014). N-n-methylene bis acrylamide: A novel fuel for combustion synthesis of zinc ferrite nanoparticles and studied by x-ray photoelectron spectroscopy. *International Journal of ChemTech Research*, 6:2834–2842.

Raman Venkatesan, T. (2022). *Tailoring applications-relevant properties in poly(vinylidene fluoride)-based homo-, co- and ter-polymers through modification of their three-phase structure*. PhD thesis.

Rani, G. J., Rajan, M., and Kumar, G. G. (2017). Reduced graphene oxide/znfe2o4 nanocomposite as an efficient catalyst for the photocatalytic degradation of methylene blue dye. *Research on Chemical Intermediates*, 43:2669–2690.

Sadighian, S. S., Abbasi, M., Arjmandi, S., and Karami, H. (2018). Dye removal from water by zinc ferrite-graphene oxide nanocomposite. *Progress in Color, Colorants and Coatings*, 11:85–92.

Sidhaarth, K., Jeyanthi, J., S., B., and . M, V. K. (2018). Adsorption of congo red dye using cobalt ferrite nanoparticles. *International Journal of Civil Engineering and Technology*, 9:1335–1347.

Singh, M., Dosanjh, H. S., and Singh, H. (2016). Surface modified spinel cobalt ferrite nanoparticles for cationic dye removal: Kinetics and thermodynamics studies. *Journal of Water Process Engineering*, 11:152–161.

SOUFI, A., HAJJAOUI, H., ELMOUBARKI, R., ABDENNOURI, M., QOURZAL, S., and BARKA, N. (2021). Spinel ferrites nanoparticles: Synthesis methods and application in heterogeneous fenton oxidation of organic pollutants – a review. *Applied Surface Science Advances*, 6:100145.

Van Uitert, L. G. (1956). Dielectric properties of and conductivity in ferrites. *Proceedings of the IRE*, 44(10):1294–1303.

Verma, M., Kumar, A., Singh, K., Kumar, R., Kumar, V., Srivastava, C., Rawat, V., Rao, G. K., Kumari, S., Sharma, P., and Kim, H. (2020). Graphene oxide-manganese ferrite (go-mnfe2o4) nanocomposite: One-pot hydrothermal synthesis and its use for adsorptive removal of pb2+ ions from aqueous medium. *Journal of Molecular Liquids*, 315:113769.

Wang, W., Chen, R., Zhao, X., Zhang, Y., Zhao, J., and Li, F. (2013). Synthesis and characteristics of superparamagnetic co0.6zn0.4fe2o4 nanoparticles by a modified hydrothermal method. *Journal of the American Ceramic Society*, 96:2245–2251.

Weng, C. and Pan, Y. (2007). Adsorption of a cationic dye (methylene blue) onto spent activated clay. *Journal of hazardous materials*, 144 1-2:355–62.

Yu, L., Sun, A., Suo, N., Zuo, Z., Zhao, X., and Zhang, W. (2020). Effect of ph on the magnetic properties and microstructure of mg0.1co0.9fe2o4 prepared by sol–gel self-propagating method. *Applied Physics A*, 126.

Zhu, Y., Murali, S., Cai, W., Li, X., Suk, J., Potts, J. R., and Ruoff, R. (2010). Graphene and graphene oxide: Synthesis, properties, and applications. *Advanced Materials*, 22.

Hieu (2018) Molla et al. (2019) Meidanchi and Ansari (2021) Deshmukh et al. (2017) Van Uitert (1956) Kuru et al. (2020) Weng and Pan (2007) Gürses et al. (2006) Lan Huong et al. (2018) Handayani et al. (2019) Mahmoodi (2013) López et al. (2021) Baynosa et al. (2020) Das et al. (2021) Singh et al. (2016) Adel et al. (2021) Jose Varghese et al. (2019) Pacakova et al. (2017) Pham et al. (2020) Naik et al. (2020) Yu et al. (2020) SOUFI et al. (2021) Marcano et al. (2010) Zhu et al. (2010) Dideikin and Vul (2019) Gerani et al. (2016) Sadighian et al. (2018) Ghobadi et al. (2018) Bayantong et al. (2021b) Katubi et al. (2021) Bayantong et al. (2021a) Fobiri (2022) Cwalinski et al. (2020) Oladoye et al. (2022) Andrei A. Bunaciu and Aboul-Enein (2015) Chen et al. (2013) Raman Venkatesan (2022) Kalantar-zadeh and Fry (2008) Verma et al. (2020) Khan et al. (2022) Wang et al. (2013) JiÅ™Ã ÄkovÃ¡ et al. (2022) Pushprajsinh H Rana (2021) Ramachandran Ph.D and Vishista (2014) Sidhaarth et al. (2018) Rani et al. (2017) Mandal et al. (2020)